



Real-time analysis of  $\delta^{13}\text{C}$ - and  $\delta\text{D-CH}_4$  in ambient air with laser spectroscopy

S. Eyer et al.

This discussion paper is/has been under review for the journal Atmospheric Measurement Techniques (AMT). Please refer to the corresponding final paper in AMT if available.

# Real-time analysis of $\delta^{13}\text{C}$ - and $\delta\text{D-CH}_4$ in ambient air with laser spectroscopy: method development and first intercomparison results

S. Eyer<sup>1</sup>, B. Tuzson<sup>1</sup>, M. E. Popa<sup>2</sup>, C. van der Veen<sup>2</sup>, T. Röckmann<sup>2</sup>, M. Rothe<sup>3</sup>, W. A. Brand<sup>3</sup>, R. Fisher<sup>4</sup>, D. Lowry<sup>4</sup>, E. G. Nisbet<sup>4</sup>, M. S. Brennwald<sup>5</sup>, E. Harris<sup>1</sup>, C. Zellweger<sup>1</sup>, L. Emmenegger<sup>1</sup>, H. Fischer<sup>6</sup>, and J. Mohn<sup>1</sup>

<sup>1</sup>Empa, Laboratory for Air Pollution & Environmental Technology, Dübendorf, Switzerland

<sup>2</sup>Utrecht University (UU), Institute for Marine and Atmospheric research Utrecht (IMAU), Utrecht, the Netherlands

<sup>3</sup>Max-Planck-Institute (MPI) for Biogeochemistry, Jena, Germany

<sup>4</sup>Royal Holloway University of London (RHUL), Department of Earth Sciences, Egham, UK

<sup>5</sup>Eawag, Water Resources and Drinking Water, Dübendorf, Switzerland

<sup>6</sup>University of Bern, Climate and Environmental Physics, Bern, Switzerland

Title Page

Abstract

Introduction

Conclusions

References

Tables

Figures



Back

Close

Full Screen / Esc

Printer-friendly Version

Interactive Discussion



Received: 30 June 2015 – Accepted: 11 August 2015 – Published: 31 August 2015

Correspondence to: J. Mohn (joachim.mohn@empa.ch)

Published by Copernicus Publications on behalf of the European Geosciences Union.

# AMTD

8, 8925–8970, 2015

## Real-time analysis of $\delta^{13}\text{C}$ - and $\delta\text{D-CH}_4$ in ambient air with laser spectroscopy

S. Eyer et al.

Title Page

Abstract

Introduction

Conclusions

References

Tables

Figures



Back

Close

Full Screen / Esc

Printer-friendly Version

Interactive Discussion



## Abstract

In situ and simultaneous measurement of the three most abundant isotopologues of methane using mid-infrared laser absorption spectroscopy is demonstrated. A field-deployable, autonomous platform is realized by coupling a compact quantum cascade laser absorption spectrometer (QCLAS) to a preconcentration unit, called TRace gas EXtractor (TREX). This unit enhances CH<sub>4</sub> mole fractions by a factor of up to 500 above ambient levels and quantitatively separates interfering trace gases such as N<sub>2</sub>O and CO<sub>2</sub>. The analytical precision of the QCLAS isotope measurement on the preconcentrated (750 ppm, parts-per-million, μmole/mole) methane is 0.1 and 0.5‰ for δ<sup>13</sup>C- and δD-CH<sub>4</sub> at 10 min averaging time.

Based on replicate measurements of compressed air during a two-week intercomparison campaign, the repeatability of the TREX-QCLAS was determined to be 0.19 and 1.9‰ for δ<sup>13</sup>C and δD-CH<sub>4</sub>, respectively. In this intercomparison campaign the new in situ technique is compared to isotope-ratio mass-spectrometry (IRMS) based on glass flask and bag sampling and real time CH<sub>4</sub> isotope analysis by two commercially available laser spectrometers. Both laser-based analyzers were limited to methane mole fraction and δ<sup>13</sup>C-CH<sub>4</sub> analysis, and only one of them, a cavity ring down spectrometer, was capable to deliver meaningful data for the isotopic composition. After correcting for scale offsets, the average difference between TREX-QCLAS data and bag/flask sampling-IRMS values are within the extended WMO compatibility goals of 0.2 and 5‰ for δ<sup>13</sup>C- and δD-CH<sub>4</sub>, respectively. Thus, the intercomparison also reveals the need for reference air samples with accurately determined isotopic composition of CH<sub>4</sub> to further improve the interlaboratory compatibility.

## 1 Introduction

Methane (CH<sub>4</sub>) is the second most important anthropogenically emitted greenhouse gas after carbon dioxide (CO<sub>2</sub>). Its mole fraction has increased from around 722 ppb

# AMTD

8, 8925–8970, 2015

## Real-time analysis of δ<sup>13</sup>C- and δD-CH<sub>4</sub> in ambient air with laser spectroscopy

S. Eyer et al.

Title Page

Abstract

Introduction

Conclusions

References

Tables

Figures



Back

Close

Full Screen / Esc

Printer-friendly Version

Interactive Discussion



**Real-time analysis of  $\delta^{13}\text{C}$ - and  $\delta\text{D-CH}_4$  in ambient air with laser spectroscopy**

S. Eyer et al.

[Title Page](#)[Abstract](#)[Introduction](#)[Conclusions](#)[References](#)[Tables](#)[Figures](#)[⏪](#)[⏩](#)[⏴](#)[⏵](#)[Back](#)[Close](#)[Full Screen / Esc](#)[Printer-friendly Version](#)[Interactive Discussion](#)

(parts-per-billion, nmole/mole) in pre-industrial times to 1824 ppb in 2013 and the anthropogenic fraction is estimated to be 60 % of the total emissions (WMO/GAW, 2014). While the tropospheric methane mole fraction and the most important sources, such as wetlands, ruminants, rice agriculture, fossil fuel production, landfills, and biomass burning, are relatively well known, considerable uncertainty remains regarding the strength and spatio-temporal variability of individual sources (Dlugokencky et al., 2011; IPCC, 2013; Manning et al., 2011; Rigby et al., 2012). A promising approach to improve the understanding of the  $\text{CH}_4$  budget is the use of isotopologues to distinguish between various  $\text{CH}_4$  source processes (Beck et al., 2012; Bergamaschi et al., 1998a; Fischer et al., 2008; Fisher et al., 2006; Nisbet et al., 2014). The isotopic composition is reported in the  $\delta$ -notation, representing the relative difference in the amount of heavy vs. light isotope of a sample in relation to an international measurement standard (Brand and Coplen, 2012; Coplen, 2011; Urey, 1948):

$$\delta^{13}\text{C} = R_{\text{sample}}/R_{\text{standard}} - 1,$$

where  $R$  represents the ratio  $[\text{}^{13}\text{CH}_4]/[\text{}^{12}\text{CH}_4]$  in the case of  $\delta^{13}\text{C}$ , and analogously  $[\text{CH}_3\text{D}]/[\text{CH}_4]$  for  $\delta\text{D}$ . The international isotopic standards are Vienna Pee Dee Belemnite (VPDB) for  $\delta^{13}\text{C}$  and Vienna Standard Mean Ocean Water (VSMOW) for  $\delta\text{D}$  (Werner and Brand, 2001). Measuring  $\delta^{13}\text{C}$ - and  $\delta\text{D-CH}_4$  is a great challenge, as the heavy isotopologues have low natural abundance, i.e. 1.1 % for  $^{13}\text{CH}_4$  and 0.06 % for  $\text{CH}_3\text{D}$  of total  $\text{CH}_4$  in the atmosphere. Nevertheless, combining the analysis of the  $\text{CH}_4$  mole fraction and its isotopic composition with inverse modelling techniques and chemical transport models has the potential to validate emission scenarios (Monteil et al., 2011). Current modelling efforts, however, are restricted by the limited continuity and temporal resolution of  $\delta^{13}\text{C-CH}_4$  measurements and the limited availability of  $\delta\text{D-CH}_4$  data (Monteil et al., 2011). This was confirmed by an observing system simulation experiment, showing significant reduction in the uncertainty of emission estimates from major national and global  $\text{CH}_4$  source categories in the case of model-generated availability of real-time high-precision measurements for  $\delta^{13}\text{C}$ - and  $\delta\text{D-CH}_4$

---

**Real-time analysis of  
 $\delta^{13}\text{C}$ - and  $\delta\text{D-CH}_4$  in  
ambient air with laser  
spectroscopy**

S. Eyer et al.

[Title Page](#)[Abstract](#)[Introduction](#)[Conclusions](#)[References](#)[Tables](#)[Figures](#)[Back](#)[Close](#)[Full Screen / Esc](#)[Printer-friendly Version](#)[Interactive Discussion](#)

data (Rigby et al., 2012). A critical requirement for such an observing system is the availability of a suitable high-precision measurement technique. Currently, IRMS is the standard technique to perform high-precision analysis of  $\delta^{13}\text{C}$ - and  $\delta\text{D-CH}_4$  in ambient air (Bock et al., 2013; Brass and Röckmann, 2010; Fischer et al., 2008; Sapart et al., 2012; Schmitt et al., 2014; Schneider et al., 2010). Being a laboratory based technique, it relies on flask sampling, which severely limits its temporal and spatial resolution capability. Furthermore, the analysis of both isotope ratios requires two separate instruments with corresponding sample preparation.

Laser spectroscopy in the mid-infrared (MIR) spectral range has emerged as a powerful alternative for the analysis of stable isotopes of  $\text{CO}_2$  (Sturm et al., 2013),  $\text{N}_2\text{O}$  (Köster et al., 2013; Mohn et al., 2012) and  $\text{CH}_4$  (Bergamaschi et al., 1994, 1998a, 1998b; Santoni et al., 2012). This development has been triggered by the invention and availability of quantum cascade lasers (QCL), which offer high optical power in continuous wave operation at room temperature (Faist, 2006; Faist et al., 2002). This enables the realization of compact, field-deployable instruments for real-time analysis at ppt (parts-per-trillion, pmole/mole) level precision (Curl et al., 2010; McManus et al., 2010). However, high-precision measurements of low abundance isotopic species of trace gases (such as  $\delta\text{D-CH}_4$ ) at ambient mole fractions require preconcentration when using direct absorption techniques (Bergamaschi et al., 1998a). The strategy of trace gas preconcentration prior to isotopic analysis by quantum cascade laser spectroscopy (QCLAS) has been demonstrated for nitrous oxide ( $\text{N}_2\text{O}$ ) isotopologues (Mohn et al., 2010, 2012) and was applied in an extended field campaign (Wolf et al., 2015).

In this paper, we present further improvements of coupling a preconcentration unit (TRace gas EXtractor, TREX) to QCLAS to achieve real-time, high-precision measurements of methane isotopic composition ( $\delta^{13}\text{C-CH}_4$ ,  $\delta\text{D-CH}_4$ ) in ambient air. We provide details on the preconcentration with TREX and present results of  $\text{CH}_4$  isotopologues analysis with QCLAS. The potential of the TREX-QCLAS technique to trace changes in ambient  $\text{CH}_4$  isotopic composition was further demonstrated in an interlaboratory comparison campaign. Results are discussed with respect to the scientifically desirable

level of compatibility between laboratories for future applications on both near-source studies and measurements of unpolluted air (WMO/GAW, 2013). Additionally, the need for whole air isotopologue reference gases with well calibrated CH<sub>4</sub> mole fraction and isotopic composition to improve compatibility of measurements performed in different laboratories is discussed.

## 2 Experimental

### 2.1 Preconcentration and analysis of CH<sub>4</sub> isotopologues by TREX-QCLAS

#### 2.1.1 Requirements for the preconcentration system

The main analytical challenge in the present work is the quantification of the CH<sub>3</sub>D isotopologue considering its very low natural abundance. A further constraint is given by the spectroscopic setup, as the same optical platform is used for simultaneous measurements of the <sup>12</sup>CH<sub>4</sub>, <sup>13</sup>CH<sub>4</sub> and CH<sub>3</sub>D isotopologues. This unavoidably involves compromises regarding the spectroscopic configuration, in particular the selected optical path length and the amount of trace gas needed to achieve the necessary measurement precision for both isotope ratios. Simulation of CH<sub>4</sub> absorption spectra in the target spectral regions indicated that optimal conditions are realized at a sample gas pressure in the range of 20 to 60 hPa and for mole fractions ranging from 600 up to 1000 ppm CH<sub>4</sub>. Since the CH<sub>4</sub> mole fraction in ambient air is generally in the order of 1.8 ppm, the TREX system had to be designed to selectively extract CH<sub>4</sub> from several liter of ambient air and concentrate into a gas volume of around 20 mL (e.g. equivalent to the amount of gas in the 0.5 L absorption cell of the laser spectrometer at a pressure of 40 hPa). In order to fulfill the above requirements, significant developments and innovative solutions for both TREX and QCLAS have been accomplished.

# AMTD

8, 8925–8970, 2015

## Real-time analysis of δ<sup>13</sup>C- and δD-CH<sub>4</sub> in ambient air with laser spectroscopy

S. Eyer et al.

Title Page

Abstract

Introduction

Conclusions

References

Tables

Figures

◀

▶

◀

▶

Back

Close

Full Screen / Esc

Printer-friendly Version

Interactive Discussion



## 2.1.2 TREX: design

The basic technology of the TREX (Fig. 1) is based on the “Medusa” system (Miller et al., 2008), which was later adopted for the preconcentration of N<sub>2</sub>O and its subsequent isotope analysis by QCLAS (Mohn et al., 2010, 2012, 2013, 2014; Waechter et al., 2008; Wolf et al., 2015). The main advantages over previously developed systems (Brand, 1995) are the low trapping temperatures in combination with its independence from liquid nitrogen. Preconcentration is achieved by temperature swing adsorption on a cold trap, filled with a specific adsorbent material. The trap is first cooled down to a temperature at which its dynamic adsorbing capacity for the target substance (here CH<sub>4</sub>) is sufficiently large, while the majority of the remaining bulk gases (e.g. N<sub>2</sub>, O<sub>2</sub>, Ar) pass through. During desorption, the trap is heated stepwise to separate the target substance from co-adsorbed interfering compounds. To minimize kinetic fractionation effects, it is important to adsorb and desorb the target substance quantitatively, i.e. with nearly 100 % recovery and with a high degree of reproducibility, as discussed below.

Given the low boiling point temperature of CH<sub>4</sub> (112 K) as an indication for its volatility, the original design of the preconcentration system required major revisions in terms of cooling power to enhance its CH<sub>4</sub> adsorption capacity. In addition, the layout was designed to fit in a compact and field-deployable 19” rack system. These two requirements led to a novel approach for the trap assembly.

Empirical investigations on the previous preconcentration unit (Mohn et al., 2010) with various trap models adsorbing CH<sub>4</sub> at different temperatures showed that for a complete and reliable CH<sub>4</sub> recovery, the amount of adsorbent material (HayeSep D, Sigma Aldrich, Switzerland) had to be increased by ten-fold. This resulted in 1.8 g of HayeSep D filled in a stainless steel tubing (length 90 cm, OD 4 mm, wall thickness 0.5 mm, volume 6.4 cm<sup>3</sup>) and bracketed with glass wool (BGB Analytics AG, Switzerland) and wired mesh. HayeSep D has previously been identified as an excellent high capacity adsorbent material for CH<sub>4</sub> (Eyer et al., 2014). The tubing is curled around a custom-made aluminum standoff with an optimized wall thickness of 0.5 mm. A ther-

## AMTD

8, 8925–8970, 2015

### Real-time analysis of $\delta^{13}\text{C}$ - and $\delta\text{D-CH}_4$ in ambient air with laser spectroscopy

S. Eyer et al.

Title Page

Abstract

Introduction

Conclusions

References

Tables

Figures

◀

▶

◀

▶

Back

Close

Full Screen / Esc

Printer-friendly Version

Interactive Discussion



# AMTD

8, 8925–8970, 2015

## Real-time analysis of $\delta^{13}\text{C}$ - and $\delta\text{D-CH}_4$ in ambient air with laser spectroscopy

S. Eyer et al.

Title Page

Abstract

Introduction

Conclusions

References

Tables

Figures



Back

Close

Full Screen / Esc

Printer-friendly Version

Interactive Discussion



mal conductance paste (340 HSC, Dow Corning Inc., USA) is applied at the contact region between trap and standoff to improve heat dissipation. To further increase the adsorption capacity of the trap, the trap temperature had to be decreased to 100 K, which was not achievable with the previous preconcentration unit. Therefore, we decided for a compact Stirling cryo-cooler with a cooling capacity of  $> 20\text{ W}$  at 100 K (CryoTel GT, Sunpower Inc., USA) gaining in terms of size, weight and performance. A copper plate disk (diameter 14 cm, weight 1.4 kg) was mounted on the cold-tip of the cooler, serving as a cold-plate with large heat capacity. Furthermore, we minimized the thermal cycle time of the trap for repeated adsorption/desorption processes through a design in which the trap is movable by a linear actuator (ZLD225MM, VG Scienta Ltd, UK). During cooling, the actuator pushes the aluminum standoff against the cold-plate. The contact pressure is adjusted to 100 N using a chromium-steel corrugated spring (WF-8941-SS, Durovis AG, Switzerland) placed between standoff and actuator. Contact surfaces between standoff and copper cold-plate are polished and coated with a thin layer of heat conductance paste (340 HSC, Dow Corning Inc., USA) to improve thermal contact. Before heating, the standoff is decoupled from the cold-plate. This approach is overall faster and yields lower trap temperatures compared to the previous preconcentration unit, because the cold plate and the Stirling cooler is completely undisturbed during the heating process.

For thermal isolation of the system, the core parts of the unit, i.e., the cold-tip of the Stirling cooler, the cold-plate, and the trap are housed in a custom-made vacuum chamber evacuated to  $< 10^{-4}$  mbar with a compact turbomolecular pump station (HiCube 80 Eco, Pfeiffer Vacuum GmbH, Switzerland). The TREX unit is controlled and monitored by a custom-developed LabVIEW program (National Instruments Corp., USA) with a graphical user interface. All peripherals are connected through a 16-port serial-to-ethernet connector (Etherlite 160, Digi International Inc., USA).



### 2.1.3 TREX: preconcentration procedure

The overall CH<sub>4</sub>-preconcentration cycle can be divided into three main phases: CH<sub>4</sub>-adsorption (phase I), CH<sub>4</sub>-desorption (phase II) and trap conditioning (phase III). At the onset of phase I, the trap is brought in contact with the cold-plate by the actuator. It takes about 15 min for the trap to cool down to a temperature of 101 K, then CH<sub>4</sub> adsorption is initiated by switching the 6-port multi-position rotary valve (Valco Instruments Inc., Switzerland) to the adsorption position as shown in Fig. 1. Dehumidified (nafion drier with dew point < 230 K, PD-50T-72MSS, Perma Pure, USA), particle-filtered (2-micron filter, SS-4FW-2, Swagelok, Switzerland) sample gas is pushed through the cooled trap with a membrane pump (PM 25032-022, KNF, Switzerland) at a pressure of 4000 hPa. The sample gas flow is adjusted downstream of the trap to a flow rate of 900 mL min<sup>-1</sup> using a mass flow controller (MFC 1, Vögtlin Instruments, Switzerland). After 500 s, corresponding to preconcentration of 7.5 L sample gas, the 6-port rotary valve is switched to the desorption position.

In phase II (CH<sub>4</sub> desorption), the linear actuator decouples the trap from the copper cold-plate with the 6-port rotary valve set to the desorption position (Fig. 1). Stepwise desorption enables quantitative separation of the target substance CH<sub>4</sub> from more volatile gases (e.g. traces of N<sub>2</sub>, O<sub>2</sub>) and less volatile trace gases, e.g. CO<sub>2</sub> and N<sub>2</sub>O. To avoid that the latter gases, which are mainly adsorbed on the front part of the trap, are released when the ends of the trap heat up, the flow direction in the desorption step is forward. The trap temperature during phase II is stepwise increased. Immediately after decoupling, its temperature increases from around 106 to 113 K without heating. Then, the trap temperature is raised first to 145 K and then to 175 K by heating with a flexible polyimide heat foil (100 W, HK5549, Minco Products Inc., USA) attached to the bottom of the aluminum standoff and controlled by a PID temperature controller (cTron, Jumo Mess- und Regeltechnik AG, Switzerland). During this period, mainly volatile bulk gases (e.g. N<sub>2</sub>, O<sub>2</sub>, Ar) with low boiling points (77 to 90 K) are desorbed from the trap and vented through the QCLAS multipass cell. The CH<sub>4</sub> desorption is

## AMTD

8, 8925–8970, 2015

### Real-time analysis of $\delta^{13}\text{C}$ - and $\delta\text{D-CH}_4$ in ambient air with laser spectroscopy

S. Eyer et al.

Title Page

Abstract

Introduction

Conclusions

References

Tables

Figures



Back

Close

Full Screen / Esc

Printer-friendly Version

Interactive Discussion





**Real-time analysis of  $\delta^{13}\text{C}$ - and  $\delta\text{D-CH}_4$  in ambient air with laser spectroscopy**

S. Eyer et al.

[Title Page](#)[Abstract](#)[Introduction](#)[Conclusions](#)[References](#)[Tables](#)[Figures](#)[◀](#)[▶](#)[◀](#)[▶](#)[Back](#)[Close](#)[Full Screen / Esc](#)[Printer-friendly Version](#)[Interactive Discussion](#)

continuous wave DFB-QCL laser (Alpes Lasers SA, Switzerland) was installed. Figure 2 shows the covered spectral range at wavenumbers of 1295.7 and 1307.0  $\text{cm}^{-1}$  selected for  $\delta^{13}\text{C}$ - and  $\delta\text{D-CH}_4$ , respectively. The spectral regions were chosen to offer maximum sensitivity for the lower abundant  $\text{CH}_3\text{D}$  isotopologues ( $\sim 10^{-22}$   $\text{cm}/\text{molecule}$   $\text{cm}^{-2}$ ), comparable line-strength for  $^{13}\text{CH}_4$  and  $^{12}\text{CH}_4$  to avoid saturation and are relatively free from spectral interferences by other molecular species. The susceptibility to spectral interferences could be further reduced by decreasing the pressure in the laser spectrometer gas cell. These conditions could not be fulfilled within the tuning capabilities of a single DFB-QCL, therefore, the simultaneous measurement of  $\delta^{13}\text{C}$ - and  $\delta\text{D-CH}_4$  required a dual-laser configuration (McManus et al., 2011). The measured absorption spectra were analyzed using commercially available software (TDLWintel, Aerodyne Research Inc., USA). In terms of precision and long-term stability, the instrument performance was characterized using the Allan variance technique (Werle, 2010).

In combination with the TREX technique the laser spectrometer is operated in a batch mode, i.e. the multipass cell is either filled with pre-concentrated sample or with calibration gas. Before each pre-concentrated sample (ambient or pressurized air), the cell is purged for two min with high-purity synthetic air at  $25 \text{ mL min}^{-1}$  flow rate and reduced pressure (8 hPa) and then evacuated to a pressure of 0.5 hPa. Similarly for the calibration gas measurements, the cell is first purged and then flushed with calibration gas dynamically diluted with high-purity synthetic air to the desired  $\text{CH}_4$  concentration at a total gas flow of  $25 \text{ mL min}^{-1}$ . The cell pressure is set to around 40 hPa ( $\pm 0.04$  hPa).

## 2.2 Interlaboratory comparison campaign

The intercomparison campaign took place from 6 to 22 June 2014 at the Empa campus, located in the densely populated area of Dübendorf, Switzerland ( $47^\circ 24' 11'' \text{ N} / 8^\circ 36' 48'' \text{ E}$ , elevation 432 m a.s.l.). A main road passes 100 m south and a highway around 750 m north of the sampling site. Air was continuously sampled from

**Real-time analysis of  $\delta^{13}\text{C}$ - and  $\delta\text{D-CH}_4$  in ambient air with laser spectroscopy**

S. Eyer et al.

[Title Page](#)[Abstract](#)[Introduction](#)[Conclusions](#)[References](#)[Tables](#)[Figures](#)[◀](#)[▶](#)[◀](#)[▶](#)[Back](#)[Close](#)[Full Screen / Esc](#)[Printer-friendly Version](#)[Interactive Discussion](#)

the rooftop of a five-story building at a flow rate of  $25 \text{ L min}^{-1}$  through a 25 m long unheated polyethylene-coated aluminum tubing (ID 9 mm, Synflex-1300) using a piston pump (Gardner Denver Thomas GmbH). At the inlet of the sampling pump the air was branched off to the different analyzers, as indicated in Fig. 3. The purpose of the campaign is to validate the TREX-QCLAS system under unattended operation conditions comparable to a “field campaign”. Flask and bag sampling as well as calibration of the commercial available laser spectrometers, however, were operated manually.

### 2.2.1 TREX-QCLAS

During the intercomparison campaign a measurement cycle of 200 min duration was applied (Fig. 4), including the measurement of three different types of calibration gases (CG 1 at 635 and 745 ppm, CG 2 at 635 ppm) as well as repeatability measurements with preconcentrated target gas (TG). This sequence allowed the measurement of up to 20 ambient air samples per day.

Raw isotope ratio measurements were at first corrected for their dependence on the laser frequency position followed by a drift correction based on regular measurements of CG 1 at 635 ppm. Calibration factors for referencing isotope ratios to the international standard scales as well as correction factors to account for the dependence of isotope ratios on  $\text{CH}_4$  mole fractions were determined by taking the mean of the calibration gas measurements in intervals of 16 to 48 h and applying a linear regression analysis. Note that the calibration gases were not preconcentrated, thus, violating the identical treatment principle. This was compensated, however, by referencing the results to pressurized ambient air (TG) measurements.

The  $\delta^{13}\text{C}$  values of preconcentrated samples were corrected for a 2.3‰ offset, which was caused by an increase in  $\text{O}_2$  mole fractions to  $40 \pm 2\%$  during preconcentration as discussed in Sect. 3.1.2. The  $\delta^{13}\text{C}$ -offset value was shown to be constant for a large range of  $\text{CH}_4$  mole fractions and the full range of  $\delta$ -values covered by this

study. For  $\delta\text{D-CH}_4$  no significant effect could be observed; most likely, its magnitude was within the uncertainty of the system.

$\text{CH}_4$  mole fractions in both ambient air and target gas were determined based on the analysis of pre-concentrated  $\text{CH}_4$  mole fractions ( $^{12}\text{CH}_4$ ), divided by the pre-concentration factor. This factor was computed for each cycle from the gas volume in the multipass cell and the volume of pre-concentrated air. The latter is derived from the sample gas flow and the adsorption time. As the trap additionally adsorbs small amounts of  $\text{N}_2$  and  $\text{O}_2$  (up to 4 % of the pre-concentrated sample volume, depending on the trap temperature), variations in the trap temperature also need to be considered. Finally, the  $\text{CH}_4$  mole fraction measurements were linked to the WMO-X2004 calibration scale (Dlugokencky et al., 2005) through calibration of the target gas against NOAA reference standards at Empa.

## 2.2.2 Commercial laser spectrometers

During the campaign, an off-axis integrated cavity output spectrometer (OA-ICOS,  $\delta^{13}\text{C-CH}_4$  and  $\text{CH}_4$  mole fraction, MCIA-24e-EP, Los Gatos Research, USA) provided by Utrecht University (UU), and a cavity ring-down spectrometer (CRDS,  $\delta^{13}\text{C-CH}_4$ ,  $\delta^{13}\text{C-CO}_2$ ,  $\text{CH}_4$  and  $\text{CO}_2$  mole fraction, G2201-I, Picarro Inc., USA) provided by Eawag, were deployed. The OA-ICOS analyzer operated in the MIR spectral region, while the CRDS instrument comprises a NIR laser source. OA-ICOS and the CRDS isotope analyzers were calibrated twice per day using the calibration gases CG 1 and CG 2 (Table 1) for 30 min each. These standards were diluted to ambient mole fractions ( $1955.3 \pm 6.8$  ppb  $\text{CH}_4$ ) with high-purity synthetic air. The dependencies of  $\delta$ -values on  $\text{CH}_4$  mole fraction were linear up to a concentration of around 2500 ppb and determined to be  $-6.35$  and  $1.18$  ‰  $\text{ppm}^{-1}$  for OA-ICOS and CRDS, respectively. They varied not significantly between beginning and end of the campaign and therefore a constant factor was applied. Thereafter, for both analyzers a drift and a two-point calibration correction for  $\delta^{13}\text{C-CH}_4$  was performed based on the measurements of CG 1 and CG 2.

# AMTD

8, 8925–8970, 2015

## Real-time analysis of $\delta^{13}\text{C-}$ and $\delta\text{D-CH}_4$ in ambient air with laser spectroscopy

S. Eyer et al.

Title Page

Abstract

Introduction

Conclusions

References

Tables

Figures

◀

▶

◀

▶

Back

Close

Full Screen / Esc

Printer-friendly Version

Interactive Discussion



Finally, 30 min averages of sample data were calculated, resulting in 550 measurement points for the CRDS over the two-week period of the intercomparison campaign. The repeatability of OA-ICOS and CRDS for  $\delta^{13}\text{C-CH}_4$  was assessed based on repeated analysis of the target gas (pressurized air) every six hours for 30 min.

### 2.2.3 Bag and flask sampling

In addition to the in situ optical analyzers, manual sampling in glass flasks and Tedlar bags for subsequent IRMS laboratory analysis was performed. Glass flasks were purged for 10 min with dehumidified ( $\text{Mg}(\text{ClO}_4)_2$ , Sigma-Aldrich, Switzerland) sample gas at  $2\text{Lmin}^{-1}$  using a membrane pump (KNF, Netherlands) and then filled to 2000 hPa. Air samples collected in glass flasks were analyzed for  $\delta^{13}\text{C-CH}_4$ ,  $\delta\text{D-CH}_4$  and  $\text{CH}_4$  mole fraction at the Institute for Marine and Atmospheric research Utrecht (IMAU) of Utrecht University (UU) and a selection of flasks were also analyzed by the Stable Isotope Laboratory of Max-Planck-Institute (MPI) for Biogeochemistry. Parallel to the glass flask sampling and through the same sample line, 3L Tedlar bags (SKC Ltd., USA) were filled and subsequently analyzed for  $\delta^{13}\text{C-CH}_4$  by IRMS and  $\text{CH}_4$  mole fraction by CRDS (G1301, Picarro Inc., USA) at the Greenhouse Gas Laboratory, Department of Earth Sciences (GGLES) of the Royal Holloway University of London (RHUL). In total, 81 flask and 48 bag samples were taken at different intervals, usually at least twice per day. Additionally, intensive sampling was performed on 13 June and from 20 June 12:00 to 22 June 12:00 (LT), when both flask and bag samples were filled every one to three hours.

### 2.2.4 IRMS analysis of $\delta^{13}\text{C-CH}_4$ and $\delta\text{D-CH}_4$ in flask samples at UU

Both  $\delta\text{D}$  and  $\delta^{13}\text{C}$  of  $\text{CH}_4$  were measured by continuous flow IRMS (ThermoFinnigan Delta plus XL) (Brass and Röckmann, 2010). First a 40 mL stainless steel (SS) sample loop is filled with sample or reference air at atmospheric pressure. The air is flushed by a flow of helium carrier gas (purity 99.9999%) to the preconcentration unit ( $1/8''$

## AMTD

8, 8925–8970, 2015

### Real-time analysis of $\delta^{13}\text{C-}$ and $\delta\text{D-CH}_4$ in ambient air with laser spectroscopy

S. Eyer et al.

Title Page

Abstract

Introduction

Conclusions

References

Tables

Figures

◀

▶

◀

▶

Back

Close

Full Screen / Esc

Printer-friendly Version

Interactive Discussion



## Real-time analysis of $\delta^{13}\text{C}$ - and $\delta\text{D-CH}_4$ in ambient air with laser spectroscopy

S. Eyer et al.

Title Page

Abstract

Introduction

Conclusions

References

Tables

Figures

⏪

⏩

⏪

⏩

Back

Close

Full Screen / Esc

Printer-friendly Version

Interactive Discussion



SS tube filled with 6 cm HayeSep D 80-100 mesh) cooled to 137 K, where the  $\text{CH}_4$  is retained and separated from the bulk air. The  $\text{CH}_4$  is released by heating the adsorbent trap to 238 K and focused in the cryo-focus unit (25 cm PoraPLOT Q, 0.32 mm ID, 117 K). For  $\delta\text{D}$  analysis the  $\text{CH}_4$  is injected (by heating the cryo-focus trap to 198 K) into a pyrolysis tube furnace (1620 K), where  $\text{CH}_4$  is converted to  $\text{H}_2$  and carbon. The  $\text{H}_2$  enters the IRMS, after passing a 2 m CarboPLOT column at room temperature (RT) and a nafion dryer, via the GasBench interface. No krypton interference could be determined in this setup. The repeatability for  $\delta\text{D-CH}_4$  is better than  $\pm 2\%$ , based on 10 consecutive analyses of standard air. A detailed inter-laboratory comparison between UU and MPI is presently ongoing and a preliminary scale offset of 4 ‰ has been used for the present evaluation.

For  $\delta^{13}\text{C}$ , the  $\text{CH}_4$  is injected from the cryo-focus unit into a combustion oven with nickel wire catalyst at  $1100^\circ\text{C}$ , where the  $\text{CH}_4$  is converted to  $\text{CO}_2$  and  $\text{H}_2\text{O}$ . The resulting gas mixture passes a nafion dryer and a 5 m PoraPLOT Q column (RT) to eliminate an interference from co-trapped krypton (Schmitt et al., 2013) before entering the IRMS via the GasBench interface. The repeatability of  $\delta^{13}\text{C}$  is better than 0.07 ‰.

### 2.2.5 IRMS analysis of $\delta^{13}\text{C-CH}_4$ and $\delta\text{D-CH}_4$ in flask samples at MPI

At the Stable Isotope Facility of MPI Jena (“BGC-IsoLab”) methane isotopes from air samples have been analyzed using a new custom made twin-mass spectrometer analysis system (Delta V+, Thermo-Fisher, Bremen, Germany) with cryogenic preconcentration and GC separation (Sperlich et al., 2013). The system allows analyzing  $\delta^{13}\text{C}$  and  $\delta\text{D}$  simultaneously in an automated and fully calibrated fashion. For every air sample, a reference air sample is analyzed concurrently. Only the difference between the reference and sample air is used for calibration. While the ion currents are analyzed on the same mass spectrometers, reference and sample air pass through dedicated cryogenic acquisition lines. The isotopic relation between these lines is established daily using four complete analyses with reference air sent through the sample preconcentration duct.

**Real-time analysis of  $\delta^{13}\text{C}$ - and  $\delta\text{D}$ - $\text{CH}_4$  in ambient air with laser spectroscopy**

S. Eyer et al.

[Title Page](#)[Abstract](#)[Introduction](#)[Conclusions](#)[References](#)[Tables](#)[Figures](#)[⏪](#)[⏩](#)[◀](#)[▶](#)[Back](#)[Close](#)[Full Screen / Esc](#)[Printer-friendly Version](#)[Interactive Discussion](#)

Using small-volume flow controllers, cryogenic acquisition is made at  $5 \text{ mL min}^{-1}$  over 20 min, thereby consuming 100 mL air for each isotope measurement. Prior to methane concentration,  $\text{CO}_2$  is removed cryogenically using a permanent liquid nitrogen bath. The cryo traps for methane retention consist of 1/8" stainless steel tubes  
5 filled with HayeSeptember-D polymer for specific absorption of  $\text{CH}_4$  at 143 K. The latter temperature is generated by compression coolers (Cryotiger, Brooks Automation, Jena, Germany), which can operate down to 123 K at a heat digestion capacity of around 30 W.

After acquisition, the acquired methane is transferred to a cryogenic focus trap of similar design, from where gas chromatographic separation is initiated by rapid heating. The methane peaks are heart cut (Deans, 1968) for combustion ( $\delta^{13}\text{C}$ ) and pyrolysis ( $\delta\text{D}$ ), respectively.  $\text{CO}_2$  is separated from non-reacted  $\text{CH}_4$  and from the co-trapped krypton with a post-reaction gas chromatographic separation before being introduced to the respective mass spectrometer via open split coupling. An entire sample carousel  
15 with 18 analyses (13 sample analyses net) takes about 27 h.

The system is in continuous operation since July 2012. The overall precision including all instrument failure times is  $\pm 0.15\text{‰}$  ( $\delta^{13}\text{C}$ ) and  $\pm 1.14\text{‰}$  ( $\delta\text{D}$ ), as determined through daily measurement of a QA (quality assurance) sample air. Removing the times of instrumental malfunction improves the precision to  $\pm 0.10\text{‰}$  ( $\delta^{13}\text{C}$ ) and  
20  $\pm 1.05\text{‰}$  ( $\delta\text{D}$ ) over the entire period of operation (3 years).

### 2.2.6 IRMS analysis of $\delta^{13}\text{C}$ - $\text{CH}_4$ in bag samples at RHUL

$\delta^{13}\text{C}$ - $\text{CH}_4$  was measured using a modified GC-IRMS system (Trace Gas and Isoprime, Isoprime Ltd.). This system uses a modified Trace Gas preparation system in dynamic mode whereby the original catalyst is replaced by palladized quartz wool in a wider  
25 4 mm ID ceramic furnace tube. Conversion of methane to  $\text{CO}_2$  and  $\text{H}_2\text{O}$  is completed at 1063 K using oxygen in the air sample as the oxidant. A highly modified and automated inlet system (Fisher et al., 2006) was applied consisting of an auto-sampler in-



## Real-time analysis of $\delta^{13}\text{C}$ - and $\delta\text{D-CH}_4$ in ambient air with laser spectroscopy

S. Eyer et al.

[Title Page](#)[Abstract](#)[Introduction](#)[Conclusions](#)[References](#)[Tables](#)[Figures](#)[Back](#)[Close](#)[Full Screen / Esc](#)[Printer-friendly Version](#)[Interactive Discussion](#)

cluding a 6-port rotary valve (Valco Instruments Inc.) with a  $75\text{ cm}^3$  Swagelok stainless steel sample volume and four samples, one standard gas and a vacuum line attached. The sample is expanded into the evacuated  $75\text{ cm}^3$  volume then pushed through the preparation system with a flow of helium gas. Individual sample analysis last approximately 19 min and all sample measurements were made in triplicate. Repeatability based on 10 consecutive analyses of standard air is  $\pm 0.05\%$  or better.  $\delta^{13}\text{C-CH}_4$  values of RHUL are offset corrected by  $-0.3\%$  based on intercomparison measurements with NIWA (Lowe, 2004).

### 2.3 Calibration gases and target gas

The calibration gases CG 1 and CG 2 were prepared at Empa based on gravimetric and dynamic dilution methods from pure fossil (99.9995 %, Messer, Switzerland) and biogenic  $\text{CH}_4$  (> 96 %, biogas plant Volketswil, Switzerland), diluted with high-purity synthetic air. Before use, the biogenic  $\text{CH}_4$  was purified from major contaminants, mainly  $\text{CO}_2$  and  $\text{H}_2\text{O}$ , by flushing it through an Ascarite/ $\text{Mg}(\text{ClO}_4)_2$  trap. The  $\delta^{13}\text{C}$  and  $\delta\text{D-CH}_4$  values of the reference gases CG 1 and CG 2, as well as of a cylinder with pressurized air used as the target gas were calibrated against the calibration scales of the Stable Isotope Laboratory of the Max-Planck-Institute (MPI) for Biogeochemistry in Jena, Germany (Sperlich et al., 2012, 2013). Results of all analytical techniques/laboratories were corrected for the offset in the target gas between assigned value determined by MPI and respective measured values.

The  $\text{CH}_4$  mole fractions of CG 1 and CG 2 were analyzed with QCLAS against commercial standards for  $\text{CH}_4$  mole fractions ( $1000 \pm 20\text{ ppmCH}_4$  in synthetic air, Messer, Switzerland), while the target gas was analyzed by WCC-Empa against the NOAA/GMD scale by CRDS (G1301, Picarro Inc., USA). Table 1 summarizes the  $\text{CH}_4$  mole fractions and  $\delta$ -values of TG, CG 1 and CG 2.

## 3 Results and discussion

### 3.1 TREX-QCLAS

#### 3.1.1 QCLAS

The QCLAS precision and stability were investigated using the Allan variance technique. Therefore, individual CH<sub>4</sub> isotopologues were measured with one second integration time over a period of a few hours, as shown in Fig. 5. From the associated Allan variance plots, an optimum averaging time of approximately 600 s can be derived, corresponding to a root mean square noise of 0.1 and 0.5‰ for δ<sup>13</sup>C-CH<sub>4</sub> and δD-CH<sub>4</sub>, respectively. The one second noise performance was determined to be in the ~ 4.0 × 10<sup>-5</sup>, which corresponds to a noise equivalent absorbance per unit path length of 5.2 × 10<sup>-9</sup> cm<sup>-1</sup> when considering the 76 m optical path.

Similar to earlier work on CO<sub>2</sub> and N<sub>2</sub>O (Tuzson et al., 2008; Waechter et al., 2008), we found also in the case of methane a linear dependence of the spectroscopically retrieved isotope ratios on the mole fractions. In a series of experiments, the magnitude of this dependence was empirically determined and verified in the range of 600–1000 ppm CH<sub>4</sub>. The coefficients were 0.0145 and -0.0521‰ ppm<sup>-1</sup> for δ<sup>13</sup>C- and δD-CH<sub>4</sub>, respectively. At each calibration phase in the intercomparison campaign, these dependencies were determined repeatedly via two-point calibration and remained stable during the two-week period.

The influence of laser temperature variation on δ<sup>13</sup>C and δD-values has been determined by systematically changing the laser heat-sink temperature over ±20 mK in steps of 3 mK, and measuring the changes observed in the retrieved isotope ratios. We found a rather strong linear dependence, i.e., 0.1 and -0.2‰ mK<sup>-1</sup> for δ<sup>13</sup>C- and δD-CH<sub>4</sub>, respectively. Thus, it was crucial not only to control the laser temperature at high-precision (≈ 1 mK), but also to record the laser temperature at high resolution and to apply a drift correction caused by this effect during data post-processing.

AMTD

8, 8925–8970, 2015

## Real-time analysis of δ<sup>13</sup>C- and δD-CH<sub>4</sub> in ambient air with laser spectroscopy

S. Eyer et al.

Title Page

Abstract

Introduction

Conclusions

References

Tables

Figures

⏪

⏩

◀

▶

Back

Close

Full Screen / Esc

Printer-friendly Version

Interactive Discussion



### 3.1.2 TREX-QCLAS

The preconcentration procedure was optimized to reduce cycle time and reach the target sample volume of 7.5 L of ambient air, but also to allow quantitative and reproducible CH<sub>4</sub>-desorption (> 99.9%) with simultaneous separation of other trace gases, such as N<sub>2</sub>O, CO<sub>2</sub> and H<sub>2</sub>O. Various trap temperatures (108 to 93 K) and gas flows (500 to 1000 mL min<sup>-1</sup>) have extensively been tested and the optimal conditions were found to be 900 mL min<sup>-1</sup> with an initial trap temperature of 101 K. Under standard operation conditions, the breakthrough volume was determined to be above 9 L of air. During this period the CH<sub>4</sub> mole fraction downstream of the trap, at the outlet of MFC 1, was below 0.5 ppb (G1301, Picarro Inc., USA).

Figure 6 displays the sequential desorption of the various compounds adsorbed on the trap. For the optimization of this procedure CH<sub>4</sub> and N<sub>2</sub>O were quantified by QCLAS, while N<sub>2</sub>, O<sub>2</sub> and CO<sub>2</sub> were measured by a quadrupole mass spectrometer (MKS, Switzerland). Quantitative (> 99.9%) CH<sub>4</sub> desorption was verified by a subsequent second desorption and analysis of the resulting effluent gas for CH<sub>4</sub>. This verifies that the tail in CH<sub>4</sub> mole fractions after the main desorption peak originates from a consecutive flushing of the QCLAS gas cell and not from CH<sub>4</sub> eluting from the trap. Within the retention time window of CH<sub>4</sub>, a fraction of O<sub>2</sub> remained on the trap is desorbed over-proportionally to N<sub>2</sub>, which leads to an increased O<sub>2</sub>-mixing ratio in the absorption cell after preconcentration in the range of 40 ± 2%. To investigate the effect of this gas matrix change on the δ-values and additional fractionation effects, calibration gases with δ<sup>13</sup>C- and δD-CH<sub>4</sub> values ranging from -36.1 to -58.5‰ and -181 to -331‰, respectively, were diluted with synthetic air to mole fractions of 2 and 2.2 ppm CH<sub>4</sub>, then preconcentrated and measured against the respective undiluted calibration gas. We observed a constant offset of 2.3 ± 0.2‰ for δ<sup>13</sup>C compared to the undiluted calibration gas, independent of CH<sub>4</sub> mole fraction or δ value. For δD no detectable influence was observed. The most plausible explanation for this effect is a change in the pressure broadening of the line profiles caused by the increased O<sub>2</sub>-mixing ratio after

## AMTD

8, 8925–8970, 2015

### Real-time analysis of δ<sup>13</sup>C- and δD-CH<sub>4</sub> in ambient air with laser spectroscopy

S. Eyer et al.

Title Page

Abstract

Introduction

Conclusions

References

Tables

Figures



Back

Close

Full Screen / Esc

Printer-friendly Version

Interactive Discussion



preconcentration. The HITRAN database contains the air pressure broadening coefficients only. Consequently, any deviation in the  $N_2/O_2$  ratio leads to a bias due to this effect, as the fitting model uses improper coefficients for line profile estimation.

In order to verify this hypothesis, we deliberately changed the gas matrix composition by setting its  $O_2$ -mole fraction to 21, 37 and 53 %. For each  $O_2$ -mixing ratio the  $CH_4$  mole fraction was increased stepwise from 600 to 1000 ppm and the  $\delta^{13}C$  dependence on  $CH_4$  mole fraction was accounted for. Figure 7 shows the measured dependence of  $\delta^{13}C-CH_4$  on changing  $O_2$ -mixing ratio. The gray bars indicate the ranges of the  $O_2$ -mixing ratio of sample gas after preconcentration as determined by mass spectrometry and the resulting offset in the  $\delta^{13}C$  values obtained for individual experiments. As mentioned before, the  $\delta D-CH_4$  values showed no significant dependence on  $O_2$ -mixing ratio.

This result confirms that the  $O_2$  interference is the main source of systematic bias for  $\delta^{13}C-CH_4$ , whereas fractionation effects for both,  $\delta^{13}C$ - and  $\delta D-CH_4$  values, are insignificant. The gas matrix effect could be reduced or at least maintained stable by enhancing the temperature control of the trap to constrain the  $O_2$ -mixing ratio in the gas matrix and thereby to improve the repeatability of  $\delta^{13}C$  measurements. Another solution could be to substitute the HayeSep D adsorbent material by a candidate either exhibiting a superior selectivity for  $CH_4$  over  $O_2$  or having a larger capacity for  $CH_4$ , so that the adsorption temperature can be increased. Higher adsorption temperatures would reduce the amount of  $O_2$  trapped in the system.

### 3.2 Repeatability of analytical techniques and scale differences between laboratories

Scale differences between different analytical techniques/laboratories and their repeatability were assessed based on repeated target gas measurements (Table 2). Figure 8 shows the histograms of the target gas measurements obtained with the TREX-QCLAS:  $CH_4$  mole fraction of  $2352.0 \pm 4.4$  ppb,  $\delta^{13}C-CH_4 = -47.99 \pm 0.19$  ‰ and  $\delta D-$

## Real-time analysis of $\delta^{13}C$ - and $\delta D-CH_4$ in ambient air with laser spectroscopy

S. Eyer et al.

Title Page

Abstract

Introduction

Conclusions

References

Tables

Figures



Back

Close

Full Screen / Esc

Printer-friendly Version

Interactive Discussion



**Real-time analysis of  $\delta^{13}\text{C}$ - and  $\delta\text{D-CH}_4$  in ambient air with laser spectroscopy**

S. Eyer et al.

Title Page

Abstract

Introduction

Conclusions

References

Tables

Figures



Back

Close

Full Screen / Esc

Printer-friendly Version

Interactive Discussion



$\text{CH}_4 = -120.9 \pm 1.9\text{‰}$ . The repeatability of TREX-QCLAS was comparable to manual sampling with subsequent IRMS analysis for  $\delta\text{D-CH}_4$ , but about a factor three worse for  $\delta^{13}\text{C-CH}_4$ . The CRDS exhibited a comparable repeatability (0.24‰) to TREX-QCLAS for  $\delta^{13}\text{C-CH}_4$ , while with 0.78‰ the performance of OA-ICOS was significantly worse.

In summary, the repeatability of TREX-QCLAS, CRDS and all IRMS laboratories offer the capability to reach the extended WMO/GAW compatibility goals for  $\delta^{13}\text{C}$  and  $\delta\text{D-CH}_4$ , of 0.2 and 5‰, defined for regional scale studies (WMO/GAW, 2013), while the goals for background measuring stations of 0.02 and 1‰ for  $\delta^{13}\text{C}$  and  $\delta\text{D-CH}_4$  are beyond the performance of any of the applied techniques. A more detailed discussion is given in Sect. 3.4.

For assessing the compatibility between the instruments, IRMS measurements of MPI were chosen as the reference point, as MPI recently established a direct link to the international isotope standard scales. The data obtained from the laser spectroscopic techniques (TREX-QCLAS, CRDS and OA-ICOS) are referenced to the standards CG 1 and CG 2, analyzed by MPI, while the IRMS measurements of UU and RHUL are referenced to their respective laboratory standards. The agreement for  $\delta^{13}\text{C-CH}_4$  is within 0.1‰ for all techniques/laboratories, except the IRMS measurements of RHUL, which were 0.25‰ higher and the OA-ICOS results, which were offset by as much as -8.87‰. For  $\delta\text{D-CH}_4$ , no significant differences were observed between TREX-QCLAS and the MPI IRMS, while the UU IRMS values were 2.3‰ higher.

The ambient air measurements during the campaign were offset-corrected for differences in  $\delta^{13}\text{C}$  and  $\delta\text{D-CH}_4$  measurements of TG by individual techniques/laboratories and MPI summarized in Table 2. Differences for IRMS laboratories include differences in scales and instrumental issues, while the laser spectroscopic techniques are all calibrated using CG 1 and CG 2. The OA-ICOS data are not considered further due to the limited performance with respect to repeatability and scale offset.

### 3.3 Real-time analysis of CH<sub>4</sub> isotopic composition in ambient air

The CH<sub>4</sub> mole fraction and isotopic composition measurements in ambient air between 6 and 22 June 2014 of the various laser spectroscopic and mass spectrometric analytical techniques is shown in Fig. 9. Data of all laboratories have been offset corrected as discussed in the previous section. During the campaign, more than 250 air samples (199 samples of ambient air, 62 target gas samples) were analyzed in stand-alone operation by TREX-QCLAS and more than 120 manually taken samples were analyzed by IRMS. The CRDS data were averaged for 30 min, resulting in 550 mean values.

The CH<sub>4</sub> mole fractions exhibit a regular diurnal variation with night-time values increasing up to 2300 ppb, which is around 400 ppb higher than at daytime. When comparing the measurement data from the local weather station in Dübendorf with the measured CH<sub>4</sub>-mole fractions, the nights with the highest emissions also exhibit very low wind speed (0–7 m s<sup>-1</sup>) and, thus, leading to more stable boundary conditions. Stable boundary conditions reduce the mixing volume of emissions, which leads to a stronger CH<sub>4</sub>-signal. Variations in the δ<sup>13</sup>C- and δD-CH<sub>4</sub> values display a clear anti-correlation with the mole fraction changes indicating emissions of CH<sub>4</sub> depleted in <sup>13</sup>CH<sub>4</sub> and CH<sub>3</sub>D. The compatibility of different techniques for CH<sub>4</sub> isotopic analysis in ambient air is discussed based on correlation diagrams in the next section.

### 3.4 Compatibility of analytical techniques for δ<sup>13</sup>C- and δD-CH<sub>4</sub> in ambient air

The compatibility of different analytical techniques for CH<sub>4</sub> isotope measurements was assessed on the ambient air measurements shown in Fig. 9. Measurements were done either on identical gas samples, i.e. for IRMS measurements of glass flask samples by UU and MPI, or on simultaneously collected ambient air samples, i.e. for all other techniques (laser spectrometers and bag samples/IRMS). The δ<sup>13</sup>C- and δD-CH<sub>4</sub> measurements on glass flasks by IRMS at UU were chosen as reference for this comparison, due to the much higher number of samples ( $n = 67$ ) analyzed as compared to MPI ( $n = 15$ ). Isotope data of all techniques were offset-corrected as described in Sect. 3.1

AMTD

8, 8925–8970, 2015

## Real-time analysis of δ<sup>13</sup>C- and δD-CH<sub>4</sub> in ambient air with laser spectroscopy

S. Eyer et al.

Title Page

Abstract

Introduction

Conclusions

References

Tables

Figures

◀

▶

◀

▶

Back

Close

Full Screen / Esc

Printer-friendly Version

Interactive Discussion





**Real-time analysis of  $\delta^{13}\text{C}$ - and  $\delta\text{D-CH}_4$  in ambient air with laser spectroscopy**

S. Eyer et al.

[Title Page](#)[Abstract](#)[Introduction](#)[Conclusions](#)[References](#)[Tables](#)[Figures](#)[Back](#)[Close](#)[Full Screen / Esc](#)[Printer-friendly Version](#)[Interactive Discussion](#)

The data were split into noon-to-noon periods and evaluated when the night-time increase in  $\text{CH}_4$  mole fractions reached above 2050 ppb. By this approach, periods with minor diurnal changes in  $\text{CH}_4$  mole fractions were excluded because the derived isotope source signatures have larger uncertainties for small mole fraction elevations. The Keeling plot approach assumes mixing of unpolluted background air with  $\text{CH}_4$  from a single source process or a constant mixture of different source processes for one noon-to-noon period. This assumption is valid for most noon-to-noon periods, as indicated by the linear regression parameters ( $R^2$ -values) being between 0.63 and 0.95 for  $\delta^{13}\text{C}$  and between 0.97 and 0.99 for  $\delta\text{D-CH}_4$ . The period from 19 to 20 June exhibited a low correlation ( $R^2 \delta^{13}\text{C}$ : 0.02,  $\delta\text{D-CH}_4$ : 0.85), caused by the contribution of various  $\text{CH}_4$  sources as discussed in the next paragraph.

In Fig. 12,  $\text{CH}_4$  isotopic source signatures for selected noon-to-noon periods are displayed. All source signatures indicate a major contribution of a microbial  $\text{CH}_4$  source process, e.g. by ruminants (Rigby et al., 2012), except the data recorded between 19 to 20 June. During this period there was a singular and pronounced emission event, with  $\text{CH}_4$  mole fractions up to 2599 ppb, suggesting significant contributions of  $\text{CH}_4$  emissions from a local fossil gas source process, which was also detected at a nearby measurement station of the Swiss Air Pollution Monitoring Network (NABEL). When ignoring this emission event, the source signature indicates a microbial source similar as in the other periods (Table 3). Unfortunately, the CRDS analyzer was in calibration mode during this event, and no flask or bag sample was collected for IRMS analysis. This event also highlights the importance of real-time  $\text{CH}_4$  isotope analysis. For the period between 21 and 22 June, source signatures obtained by TREX-QCLAS were compared to the IRMS results by UU and MPI of glass flask sampling and the agreement is within the expanded uncertainty of the linear regression (Table 3).

The measurements made during this campaign clearly demonstrate that the TREX-QCLAS technique is a valuable attractive alternative to the existing laboratory-based techniques that rely on flask sampling. Moreover, the TREX-QCLAS is capable to resolve temporal changes in ambient  $\text{CH}_4$  isotopic composition. Finally, the preconcentration





tion, the TREX-QCLAS is perfectly suited for field studies at ecosystem measurement sites in order to identify regional source processes.

*Acknowledgements.* Funding from the Swiss National Science Foundation (SNSF) within grant No. 200021\_134611 and the European Community's Seventh Framework Programme (FP7/2007-2013) within the InGOS project under grant agreement No. 284274 is gratefully acknowledged. We thank Biogas Volketswil for providing us with pure biogenic CH<sub>4</sub>. S. Eyer is very thankful for the continuous support from the electronic (W. Knecht and A. Kunz) and mechanic (U. Hintermüller and E. Pieper) workshops at Empa. In addition we would like to thank Kerstin Zeyer, Antoine Roth and Marco Weber (Empa) for their support. M. E. Popa travel to Dübendorf was supported by the COST ACTION MP1204 TERA-MIR.

## References

- Beck, V., Chen, H., Gerbig, C., Bergamaschi, P., Bruhwiler, L., Houweling, S., Röckmann, T., Kolle, O., Steinbach, J., Koch, T., Sapart, C. J., Van Der Veen, C., Frankenberg, C., Andreae, M. O., Artaxo, P., Longo, K. M., and Wofsy, S. C.: Methane airborne measurements and comparison to global models during BARCA, *J. Geophys. Res.-Atmos.*, 117, D15310, doi:10.1029/2011JD017345, 2012.
- Bergamaschi, P., Schupp, M., and Harris, G. W.: High-precision direct measurements of <sup>13</sup>CH<sub>4</sub>/<sup>12</sup>CH<sub>4</sub> and <sup>12</sup>CH<sub>3</sub>D/<sup>12</sup>CH<sub>4</sub> ratios in atmospheric methane sources by means of a long-path tunable diode laser absorption spectro, *Appl. Optics*, 33, 7704–7716, doi:10.1364/AO.33.007704, 1994.
- Bergamaschi, P., Brenninkmeijer, C. A. M., Hahn, M., Röckmann, T., Scharffe, D. H., Crutzen, P. J., Elansky, N. F., Belikov, I. B., Trivett, N. B. A., and Worthy, D. E. J.: Isotope analysis based source identification for atmospheric CH<sub>4</sub> and CO sampled across Russia using the Trans-Siberian railroad, *J. Geophys. Res.*, 103, 8227, doi:10.1029/97JD03738, 1998a.
- Bergamaschi, P., Lubina, C., Königstedt, R., Fischer, H., Veltkamp, A. C., and Zwaagstra, O.: Stable isotopic signatures (δ<sup>13</sup>C, δD) of methane from European landfill sites, *J. Geophys. Res.*, 103, 8251–8265, doi:10.1029/98JD00105, 1998b.
- Bock, M., Schmitt, J., Beck, J., Schneider, R., and Fischer, H.: Improving accuracy and precision of ice core δD(CH<sub>4</sub>) analyses using methane pre-pyrolysis and hydrogen post-pyrolysis

## Real-time analysis of δ<sup>13</sup>C- and δD-CH<sub>4</sub> in ambient air with laser spectroscopy

S. Eyer et al.

Title Page

Abstract

Introduction

Conclusions

References

Tables

Figures



Back

Close

Full Screen / Esc

Printer-friendly Version

Interactive Discussion



## Real-time analysis of $\delta^{13}\text{C}$ - and $\delta\text{D-CH}_4$ in ambient air with laser spectroscopy

S. Eyer et al.

Title Page

Abstract

Introduction

Conclusions

References

Tables

Figures



Back

Close

Full Screen / Esc

Printer-friendly Version

Interactive Discussion



trapping and subsequent chromatographic separation, *Atmos. Meas. Tech.*, 7, 1999–2012, doi:10.5194/amt-7-1999-2014, 2014.

Brand, W. A.: PreCon: a fully automated interface for the pre-GC concentration of trace gases on air for isotopic analysis, *Isot. Environ. Healt. S.*, 31, 277–284, doi:10.1080/10256019508036271, 1995.

Brand, W. A. and Coplen, T. B.: Stable isotope deltas: tiny, yet robust signatures in nature, *Isot. Environ. Healt. S.*, 48, 393–409, doi:10.1080/10256016.2012.666977, 2012.

Brass, M. and Röckmann, T.: Continuous-flow isotope ratio mass spectrometry method for carbon and hydrogen isotope measurements on atmospheric methane, *Atmos. Meas. Tech.*, 3, 1707–1721, doi:10.5194/amt-3-1707-2010, 2010.

Coplen, T. B.: Guidelines and recommended terms for expression of stable-isotope-ratio and gas-ratio measurement results., *Rapid Commun. Mass Sp.*, 25, 2538–2560, doi:10.1002/rcm.5129, 2011.

Curl, R. F., Capasso, F., Gmachl, C., Kosterev, A. A., McManus, J. B., Lewicki, R., Pusharsky, M., Wysocki, G., and Tittel, F. K.: Quantum cascade lasers in chemical physics, *Chem. Phys. Lett.*, 487, 1–18, doi:10.1016/j.cplett.2009.12.073, 2010.

Deans, D. R.: A new technique for heart cutting in gas chromatography [1], *Chromatographia*, 1, 18–22, doi:10.1007/BF02259005, 1968.

Dlugokencky, E. J., Myers, R. C., Lang, P. M., Masarie, K. A., Crotwell, A. M., Thoning, K. W., Hall, B. D., Elkins, J. W., and Steele, L. P.: Conversion of NOAA atmospheric dry air  $\text{CH}_4$  mole fractions to a gravimetrically prepared standard scale, *J. Geophys. Res.-Atmos.*, 110, 1–8, doi:10.1029/2005JD006035, 2005.

Dlugokencky, E. J., Nisbet, E. G., Fisher, R., and Lowry, D.: Global atmospheric methane: budget, changes and dangers, *Philos. T. Roy. Soc. A.*, 369, 2058–2072, doi:10.1098/rsta.2010.0341, 2011.

Eyer, S., Stadie, N. P., Borgschulte, A., Emmenegger, L., and Mohn, J.: Methane preconcentration by adsorption: a methodology for materials and conditions selection, *Adsorption*, 20, 657–666, doi:10.1007/s10450-014-9609-9, 2014.

Faist, J.: Continuous-wave, room-temperature quantum cascade lasers, *Opt. Photonics News*, 17, 32–36, doi:10.1364/OPN.17.5.000032, 2006.

Faist, K., Hofstetter, D., Beck, M., Aellen, T., Rochat, M., and Blaser, S.: Bound-to-continuum and two-phonon resonance, quantum-cascade lasers for high duty cycle, high-temperature operation, *IEEE J. Quantum Elect.*, 38, 533–546, doi:10.1109/JQE.2002.1005404, 2002.

## Real-time analysis of $\delta^{13}\text{C}$ - and $\delta\text{D-CH}_4$ in ambient air with laser spectroscopy

S. Eyer et al.

Title Page

Abstract

Introduction

Conclusions

References

Tables

Figures

◀

▶

◀

▶

Back

Close

Full Screen / Esc

Printer-friendly Version

Interactive Discussion



Fischer, H., Behrens, M., Bock, M., Richter, U., Schmitt, J., Loulergue, L., Chappellaz, J., Spahni, R., Blunier, T., Leuenberger, M., and Stocker, T. F.: Changing boreal methane sources and constant biomass burning during the last termination, *Nature*, 452, 864–867, doi:10.1038/nature06825, 2008.

5 Fisher, R., Lowry, D., Wilkin, O., Sriskantharajah, S., and Nisbet, E. G.: High-precision, automated stable isotope analysis of atmospheric methane and carbon dioxide using continuous-flow isotope-ratio mass spectrometry, *Rapid Commun. Mass Sp.*, 20, 200–208, doi:10.1002/rcm.2300, 2006.

10 IPCC: Climate Change 2013: the Physical Science Basis. Contribution of Working Group I to the Fifth Assessment Report of the Intergovernmental Panel on Climate Change, edited by: Stocker, T. F., Qin, D., Plattner, G.-K., Tignor, M., Allen, S. K., Boschung, J., Nauels, A., Xia, Y., Bex, V., and Midgley, P. M., Cambridge University Press, Cambridge, United Kingdom and New York, NY, USA, 1535 pp., doi:10.1017/CBO9781107415324, 2013.

15 Keeling, C. D.: The concentration and isotopic abundances of atmospheric carbon dioxide in rural areas, *Geochim. Cosmochim. Ac.*, 13, 322–334, doi:10.1016/0016-7037(58)90033-4, 1958.

Keeling, C. D.: The concentration and isotopic abundances of carbon dioxide in rural and marine air, *Geochim. Cosmochim. Ac.*, 24, 277–298, doi:10.1016/0016-7037(61)90023-0, 1961.

20 Köster, J. R., Well, R., Tuzson, B., Bol, R., Dittert, K., Giesemann, A., Emmenegger, L., Manninen, A., Cárdenas, L., and Mohn, J.: Novel laser spectroscopic technique for continuous analysis of  $\text{N}_2\text{O}$  isotopomers – application and intercomparison with isotope ratio mass spectrometry, *Rapid Commun. Mass Sp.*, 27, 216–222, doi:10.1002/rcm.6434, 2013.

Lowe, D. C.: Seasonal cycles of mixing ratio and  $^{13}\text{C}$  in atmospheric methane at Suva, Fiji, *J. Geophys. Res.*, 109, D23308, doi:10.1029/2004JD005166, 2004.

25 Manning, A. C., Nisbet, E. G., Keeling, R. F., and Liss, P. S.: Greenhouse gases in the Earth system: setting the agenda to 2030, *Philos. T. Roy. Soc. A.*, 369, 1885–1890, doi:10.1098/rsta.2011.0076, 2011.

McManus, J. B., Zahniser, M. S., Nelson, D. D., Shorter, J. H., Herndon, S., Wood, E., and Wehr, R.: Application of quantum cascade lasers to high-precision atmospheric trace gas measurements, *Opt. Eng.*, 49, 111124, 1–11, doi:10.1117/1.3498782, 2010.

30 McManus, J. B., Zahniser, M. S., and Nelson, D. D.: Dual quantum cascade laser trace gas instrument with astigmatic Herriott cell at high pass number, *Appl. Optics*, 50, A74–A85, doi:10.1364/AO.50.000A74, 2011.

**Real-time analysis of  $\delta^{13}\text{C}$ - and  $\delta\text{D-CH}_4$  in ambient air with laser spectroscopy**

S. Eyer et al.

Title Page

Abstract

Introduction

Conclusions

References

Tables

Figures



Back

Close

Full Screen / Esc

Printer-friendly Version

Interactive Discussion



- Miller, B. R., Weiss, R. F., Salameh, P. K., Tanhua, T., Grealley, B. R., Mühle, J., and Simmonds, P. G.: Medusa: a sample preconcentration and GC/MS detector system for in situ measurements of atmospheric trace halocarbons, hydrocarbons, and sulfur compounds, *Anal. Chem.*, 80, 1536–1545, doi:10.1021/ac702084k, 2008.
- 5 Mohn, J., Guggenheim, C., Tuzson, B., Vollmer, M. K., Toyoda, S., Yoshida, N., and Emmenegger, L.: A liquid nitrogen-free preconcentration unit for measurements of ambient  $\text{N}_2\text{O}$  isotopomers by QCLAS, *Atmos. Meas. Tech.*, 3, 609–618, doi:10.5194/amt-3-609-2010, 2010.
- Mohn, J., Tuzson, B., Manninen, A., Yoshida, N., Toyoda, S., Brand, W. A., and Emmenegger, L.: Site selective real-time measurements of atmospheric  $\text{N}_2\text{O}$  isotopomers by laser spectroscopy, *Atmos. Meas. Tech.*, 5, 1601–1609, doi:10.5194/amt-5-1601-2012, 2012.
- 10 Mohn, J., Steinlin, C., Merbold, L., Emmenegger, L., and Hagedorn, F.:  $\text{N}_2\text{O}$  emissions and source processes in snow-covered soils in the Swiss Alps, *Isot. Environ. Health. S.*, 49, 520–531, doi:10.1080/10256016.2013.826212, 2013.
- Mohn, J., Wolf, B., Toyoda, S., Lin, C.-T., Liang, M.-C., Brüggemann, N., Wissel, H., Steiker, A. E., Dyckmans, J., Szwece, L., Ostrom, N. E., Casciotti, K. L., Forbes, M., Giese-  
mann, A., Well, R., Doucett, R. R., Yarnes, C. T., Ridley, A. R., Kaiser, J., and Yoshida, N.: Interlaboratory assessment of nitrous oxide isotopomer analysis by isotope ratio mass spec-  
trometry and laser spectroscopy: current status and perspectives, *Rapid Commun. Mass Sp.*, 28, 1995–2007, doi:10.1002/rcm.6982, 2014.
- 20 Monteil, G., Houweling, S., Dlugokenky, E. J., Maenhout, G., Vaughn, B. H., White, J. W. C., and Rockmann, T.: Interpreting methane variations in the past two decades using measurements of  $\text{CH}_4$  mixing ratio and isotopic composition, *Atmos. Chem. Phys.*, 11, 9141–9153, doi:10.5194/acp-11-9141-2011, 2011.
- Nisbet, E. G., Dlugokenky, E. J., and Bousquet, P.: Methane on the rise-again, *Science*, 343, 493–495, doi:10.1126/science.1247828, 2014.
- 25 Rigby, M., Manning, A. J., and Prinn, R. G.: The value of high-frequency, high-precision methane isotopologue measurements for source and sink estimation, *J. Geophys. Res.-Atmos.*, 117, D12312, doi:10.1029/2011JD017384, 2012.
- Santoni, G. W., Lee, B. H., Goodrich, J. P., Varner, R. K., Crill, P. M., McManus, J. B., Nelson, D. D., Zahniser, M. S., and Wofsy, S. C.: Mass fluxes and isofluxes of methane ( $\text{CH}_4$ ) at a New Hampshire fen measured by a continuous wave quantum cascade laser spectrom-  
eter, *J. Geophys. Res.-Atmos.*, 117, D10301, doi:10.1029/2011JD016960, 2012.
- 30

## Real-time analysis of $\delta^{13}\text{C}$ - and $\delta\text{D-CH}_4$ in ambient air with laser spectroscopy

S. Eyer et al.

[Title Page](#)
[Abstract](#)
[Introduction](#)
[Conclusions](#)
[References](#)
[Tables](#)
[Figures](#)




[Back](#)
[Close](#)
[Full Screen / Esc](#)
[Printer-friendly Version](#)
[Interactive Discussion](#)


Sapart, C. J., Monteil, G., Prokopiou, M., van de Wal, R. S. W., Kaplan, J. O., Sperlich, P., Krumhardt, K. M., van der Veen, C., Houweling, S., Krol, M. C., Blunier, T., Sowers, T., Martinerie, P., Witrant, E., Dahl-Jensen, D., and Röckmann, T.: Natural and anthropogenic variations in methane sources during the past two millennia, *Nature*, 490, 85–88, doi:10.1038/nature11461, 2012.

Schmitt, J., Seth, B., Bock, M., van der Veen, C., Möller, L., Sapart, C. J., Prokopiou, M., Sowers, T., Röckmann, T., and Fischer, H.: On the interference of Kr during carbon isotope analysis of methane using continuous-flow combustion–isotope ratio mass spectrometry, *Atmos. Meas. Tech.*, 6, 1425–1445, doi:10.5194/amt-6-1425-2013, 2013.

Schmitt, J., Seth, B., Bock, M., and Fischer, H.: Online technique for isotope and mixing ratios of  $\text{CH}_4$ ,  $\text{N}_2\text{O}$ , Xe and mixing ratios of organic trace gases on a single ice core sample, *Atmos. Meas. Tech.*, 7, 2645–2665, doi:10.5194/amt-7-2645-2014, 2014.

Schneider, R., Bock, M., Schmitt, J., Behrens, M., Mo, L., Sapart, C., and Fischer, H.: A gas chromatography/pyrolysis/isotope ratio mass spectrometry system for high-precision  $\delta\text{D}$  measurements of atmospheric methane extracted from ice cores, *Rapid Commun. Mass Sp.*, 24, 621–633, doi:10.1002/rcm.4429, 2010.

Sperlich, P., Guillevic, M., Buizert, C., Jenk, T. M., Sapart, C. J., Schaefer, H., Popp, T. J., and Blunier, T.: A combustion setup to precisely reference  $\delta^{13}\text{C}$  and  $\delta^2\text{H}$  isotope ratios of pure  $\text{CH}_4$  to produce isotope reference gases of  $\delta^{13}\text{C-CH}_4$  in synthetic air, *Atmos. Meas. Tech.*, 5, 2227–2236, doi:10.5194/amt-5-2227-2012, 2012.

Sperlich, P., Buizert, C., Jenk, T. M., Sapart, C. J., Prokopiou, M., Röckmann, T., and Blunier, T.: An automated GC-C-GC-IRMS setup to measure palaeoatmospheric  $\delta^{13}\text{C-CH}_4$ ,  $\delta^{15}\text{N-N}_2\text{O}$  and  $\delta^{18}\text{O-N}_2\text{O}$  in one ice core sample, *Atmos. Meas. Tech.*, 6, 2027–2041, doi:10.5194/amt-6-2027-2013, 2013.

Sturm, P., Tuzson, B., Henne, S., and Emmenegger, L.: Tracking isotopic signatures of  $\text{CO}_2$  at the high altitude site Jungfrauoch with laser spectroscopy: analytical improvements and representative results, *Atmos. Meas. Tech.*, 6, 1659–1671, doi:10.5194/amt-6-1659-2013, 2013.

Tuzson, B., Mohn, J., Zeeman, M. J., Werner, R. A., Eugster, W., Zahniser, M. S., Nelson, D. D., McManus, J. B., and Emmenegger, L.: High precision and continuous field measurements of  $\delta^{13}\text{C}$  and  $\delta^{18}\text{O}$  in carbon dioxide with a cryogen-free QCLAS, *Appl. Phys. B*, 92, 451–458, doi:10.1007/s00340-008-3085-4, 2008.

## Real-time analysis of $\delta^{13}\text{C}$ - and $\delta\text{D-CH}_4$ in ambient air with laser spectroscopy

S. Eyer et al.

[Title Page](#)
[Abstract](#)
[Introduction](#)
[Conclusions](#)
[References](#)
[Tables](#)
[Figures](#)
[Back](#)
[Close](#)
[Full Screen / Esc](#)
[Printer-friendly Version](#)
[Interactive Discussion](#)


Tuzson, B., Hiller, R. V., Zeyer, K., Eugster, W., Neftel, A., Ammann, C., and Emmenegger, L.: Field intercomparison of two optical analyzers for  $\text{CH}_4$  eddy covariance flux measurements, *Atmos. Meas. Tech.*, 3, 1519–1531, doi:10.5194/amt-3-1519-2010, 2010.

Urey, H. C.: Oxygen isotopes in nature and in the laboratory, *Science*, 108, 489–496, doi:10.1126/science.108.2810.489, 1948.

Waechter, H., Mohn, J., Tuzson, B., Emmenegger, L., and Sigrist, M. W.: Determination of  $\text{N}_2\text{O}$  isotopomers with quantum cascade laser based absorption spectroscopy, *Opt. Express*, 16, 9239–9244, doi:10.1364/OE.16.009239, 2008.

Werle, P.: Accuracy and precision of laser spectrometers for trace gas sensing in the presence of optical fringes and atmospheric turbulence, *Appl. Phys. B*, 102, 313–329, doi:10.1007/s00340-010-4165-9, 2010.

Werner, R. and Brand, W.: Referencing strategies and techniques in stable isotope ratio analysis., *Rapid Commun. Mass Sp.*, 15, 501–519, doi:10.1002/rcm.258, 2001.

WMO/GAW: GAW Report No. 213 17th WMO/IAEA Meeting on Carbon Dioxide, Other Greenhouse Gases and Related Tracers Measurement Techniques (GGMT-2013), Beijing, available at: <http://www.wmo.int/pages/prog/arep/gaw/gaw-reports.html>, 2014.

WMO/GAW: WMO Greenhouse Gas Bulletin, available at: [http://www.wmo.int/pages/prog/arep/gaw/ghg/documents/GHG\\_Bulletin\\_10\\_Nov2014\\_EN.pdf](http://www.wmo.int/pages/prog/arep/gaw/ghg/documents/GHG_Bulletin_10_Nov2014_EN.pdf), 2014.

Wolf, B., Merbold, L., Decock, C., Tuzson, B., Harris, E., Six, J., Emmenegger, L., and Mohn, J.: First on-line isotopic characterization of  $\text{N}_2\text{O}$  above intensively managed grassland, *Biogeosciences*, 12, 2517–2531, doi:10.5194/bg-12-2517-2015, 2015.

## Real-time analysis of $\delta^{13}\text{C}$ - and $\delta\text{D-CH}_4$ in ambient air with laser spectroscopy

S. Eyer et al.

Title Page

Abstract

Introduction

Conclusions

References

Tables

Figures

◀

▶

◀

▶

Back

Close

Full Screen / Esc

Printer-friendly Version

Interactive Discussion



**Table 1.** List of  $\text{CH}_4$  mole fractions and isotopic composition ( $\delta^{13}\text{C}$  and  $\delta\text{D-CH}_4$ ) of laboratory standards used in the intercomparison campaign. The indicated uncertainty is the  $1\sigma$  standard deviation for repeated analysis of the respective measurement system.

	composition	$\text{CH}_4$ [ppm]	$\delta^{13}\text{C-CH}_4^c$ [‰]	$\delta\text{D-CH}_4^c$ [‰]
CG 1	fossil/biogenic $\text{CH}_4$ in synthetic air	$938.8 \pm 3.5^a$	$-46.60 \pm 0.10$	$-250.46 \pm 1.05$
CG 2	fossil $\text{CH}_4$ in synthetic air	$1103.8 \pm 3.5^a$	$-36.13 \pm 0.10$	$-180.58 \pm 1.05$
TG	pressurized ambient air	$2.3523 \pm 0.0002^b$	$-48.07 \pm 0.10$	$-120.00 \pm 1.05$

$\text{CH}_4$  mole fractions were measured by CRDS<sup>a</sup> after dilution by a factor of 1 : 500 or<sup>b</sup> by direct measurement.

<sup>c</sup> Isotopic values were analyzed by IRMS at MPI.



## Real-time analysis of $\delta^{13}\text{C}$ - and $\delta\text{D-CH}_4$ in ambient air with laser spectroscopy

S. Eyer et al.

Title Page

Abstract

Introduction

Conclusions

References

Tables

Figures

◀

▶

◀

▶

Back

Close

Full Screen / Esc

Printer-friendly Version

Interactive Discussion



**Table 2.** List of measured  $\delta^{13}\text{C-CH}_4$  and  $\delta\text{D-CH}_4$  values of the target gas (pressurized air) as reported by different analytical techniques/laboratories. The indicated uncertainty is the  $1\sigma$  standard deviation. Results of laser spectroscopic techniques are referenced to standards CG 1 and CG 2, while IRMS results where referenced to their respective laboratory standards.

	number of measurements	$\delta^{13}\text{C-CH}_4$ [‰]	$\delta\text{D-CH}_4$ [‰]
Glass-flask/IRMS (MPI)	1	$-48.07 \pm 0.10$	$-120.0 \pm 1.05$
TREX-QCLAS (Empa)	62	$-47.99 \pm 0.19$	$-120.9 \pm 1.9$
Glass-flask/IRMS (UU)	4	$-47.96 \pm 0.08$	$-117.7 \pm 2.0$
CRDS (Eawag)	64	$-48.04 \pm 0.24$	n.a.
OA-ICOS (UU)	10	$-56.94 \pm 0.78$	n.a.
Bag/IRMS (RHUL)	3	$-47.82 \pm 0.05$	n.a.

n.a.: not analyzed.

## Real-time analysis of $\delta^{13}\text{C}$ - and $\delta\text{D-CH}_4$ in ambient air with laser spectroscopy

S. Eyer et al.

**Table 3.** Overview of all the  $\delta^{13}\text{C-CH}_4$  and  $\delta\text{D-CH}_4$  source signatures derived using the Keeling plot approach for the given time periods.

System	Time period (12:00–12:00)	#Points	$\text{CH}_4^{\text{Max}}$ ppb	$\delta^{13}\text{C-CH}_4$ [‰]	$\delta\text{D-CH}_4$ [‰]	$R^2\text{-}\delta\text{D}$	$R^2\text{-}\delta^{13}\text{C}$
TREX-QCLAS	7–8 Jun 2014	18	2222	$-55.1 \pm 1.2$	$-368 \pm 13$	0.72	0.97
TREX-QCLAS	8–9 Jun 2014	18	2308	$-57.9 \pm 0.6$	$-351 \pm 7$	0.95	0.99
TREX-QCLAS	18–19 Jun 2014	18	2208	$-57.2 \pm 1.3$	$-344 \pm 12$	0.78	0.97
TREX-QCLAS	19–20 Jun 2014 <sup>a</sup>	17	2599	$-49.7 \pm 2.1$	$-264 \pm 18$	0.02	0.85
TREX-QCLAS	19–20 Jun 2014 <sup>b</sup>	16	2176	$-61.5 \pm 1.3$	$-372 \pm 12$	0.89	0.97
TREX-QCLAS	21–22 Jun 2014	15	2067	$-55.4 \pm 1.7$	$-374 \pm 12$	0.63	0.98
IRMS UU	21–22 Jun 2014	10	2072	$-52.4 \pm 1.9$	$-351 \pm 19$	0.34	0.94
IRMS MPI	21–22 Jun 2014	6	2072	$-54.7 \pm 1.9$	$-356 \pm 20$	0.74	0.98

Values from the period between 19 and 20 June were derived with <sup>a</sup> and without <sup>b</sup> consideration of the event data point.

Title Page

Abstract

Introduction

Conclusions

References

Tables

Figures

⏪

⏩

◀

▶

Back

Close

Full Screen / Esc

Printer-friendly Version

Interactive Discussion



## Real-time analysis of $\delta^{13}\text{C}$ - and $\delta\text{D-CH}_4$ in ambient air with laser spectroscopy

S. Eyer et al.

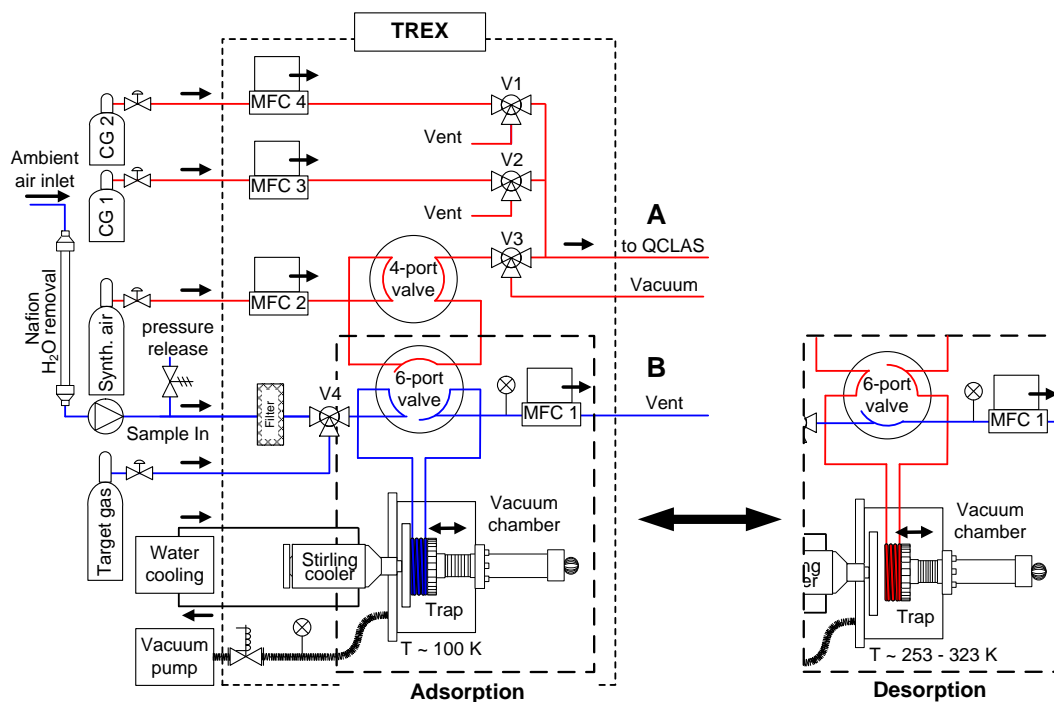


**Figure 1.** Schematics of the preconcentration unit (TREX). The blue lines indicate the flow of sample air and TG, i.e. ambient air  $\text{CH}_4$ -mole fractions, while red lines represent the flow of calibration gases and desorbed air, i.e. high  $\text{CH}_4$ -mole fraction. MFC 1-4 and V1-4 stand for mass flow controllers and 2-position valves, respectively.

Title Page

Abstract

Introduction

Conclusions

References

Tables

Figures

◀

▶

◀

▶

Back

Close

Full Screen / Esc

Printer-friendly Version

Interactive Discussion

## Real-time analysis of $\delta^{13}\text{C}$ - and $\delta\text{D}$ - $\text{CH}_4$ in ambient air with laser spectroscopy

S. Eyer et al.

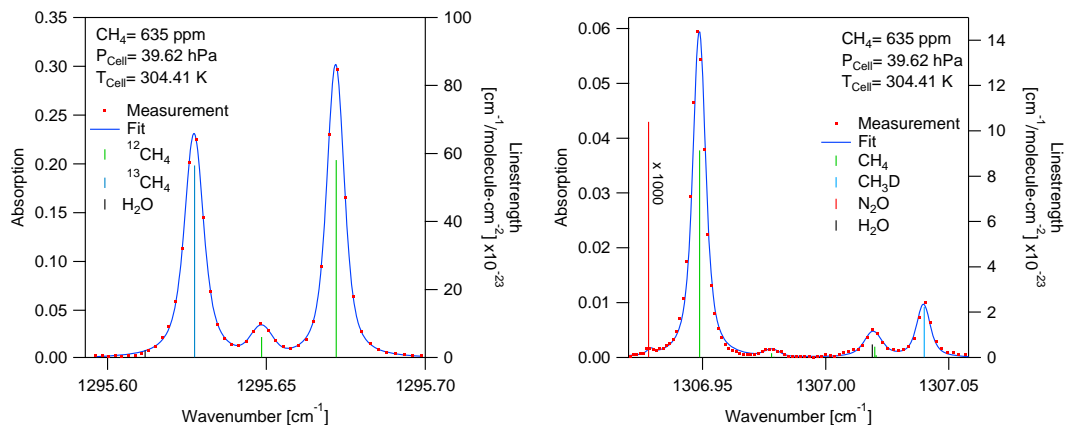


**Figure 2.** Measured absorption spectra for the determination of  $\delta^{13}\text{C}$ - (left) and  $\delta\text{D}$ - $\text{CH}_4$  (right) along with the spectral fit using Voigt-profiles and the corresponding line-strengths from the HITRAN database. Potential interferences are expected mainly from  $\text{N}_2\text{O}$  and  $\text{H}_2\text{O}$ . The spectral line of  $\text{N}_2\text{O}$  is divided by a factor of 1000 to fit in the graph, evidencing that even  $\text{N}_2\text{O}$ -mole fraction of around 300 ppb can cause severe interference.

Title Page

Abstract

Introduction

Conclusions

References

Tables

Figures

◀

▶

◀

▶

Back

Close

Full Screen / Esc

Printer-friendly Version

Interactive Discussion



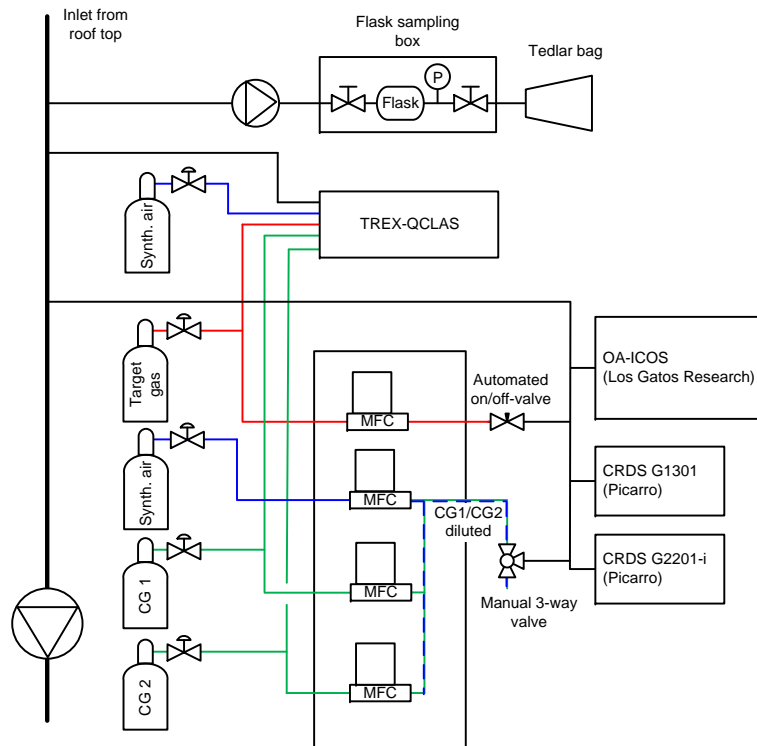


**Figure 3.** Schematics of the sampling setup used in the interlaboratory comparison campaign. Ambient air was continuously sampled from the rooftop of the building, and split from the main line to the batch sampling unit (bags and flasks), to the TREX-QCLAS system and to the continuous flow CRDS and OA-ICOS spectrometers. The laser spectrometers were additionally supplied with the calibration gases CG 1, CG 2 and the target gas to determine calibration factors and repeatability.

## Real-time analysis of $\delta^{13}\text{C}$ - and $\delta\text{D-CH}_4$ in ambient air with laser spectroscopy

S. Eyer et al.

Title Page

Abstract

Introduction

Conclusions

References

Tables

Figures

◀

▶

◀

▶

Back

Close

Full Screen / Esc

Printer-friendly Version

Interactive Discussion



**Real-time analysis of  $\delta^{13}\text{C}$ - and  $\delta\text{D}$ - $\text{CH}_4$  in ambient air with laser spectroscopy**

S. Eyer et al.

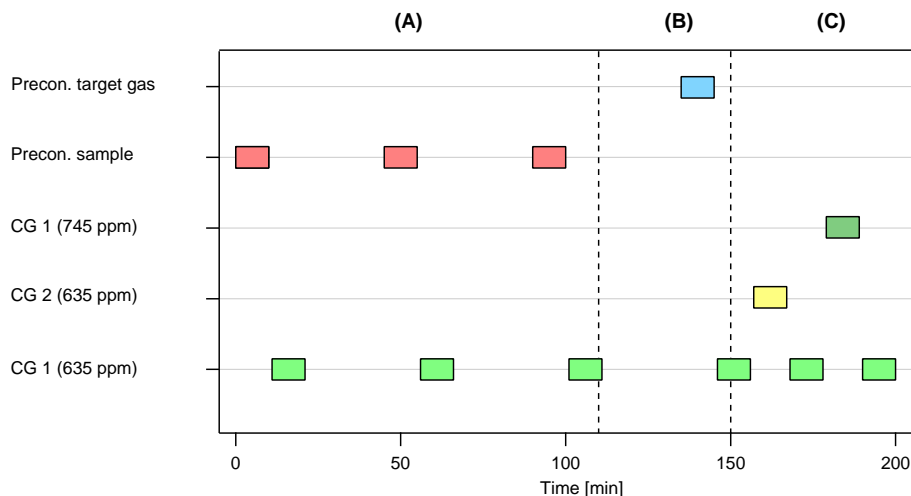


**Figure 4.** A complete measurement cycle consist of three main sequences: (A) three consecutive measurements of preconcentrated ambient air samples, (B) one measurement of preconcentrated pressurized air (target gas), followed by the calibration phase (C). The latter is used for the determination of calibration factors for  $\delta^{13}\text{C}$ - $\text{CH}_4$  and  $\delta\text{D}$ - $\text{CH}_4$  and the dependence of isotope ratios on elevated  $\text{CH}_4$  mole fractions. The calibration gases are dynamically diluted to the indicated  $\text{CH}_4$  mole fractions as described in Sect. 2.2.1. All measurements are bracketed by the analysis of CG 1 (anchor) at 635 ppm  $\text{CH}_4$  to drift-correct the measurements.

Title Page

Abstract

Introduction

Conclusions

References

Tables

Figures

◀

▶

◀

▶

Back

Close

Full Screen / Esc

Printer-friendly Version

Interactive Discussion



**Real-time analysis of  $\delta^{13}\text{C}$ - and  $\delta\text{D}$ - $\text{CH}_4$  in ambient air with laser spectroscopy**

S. Eyer et al.

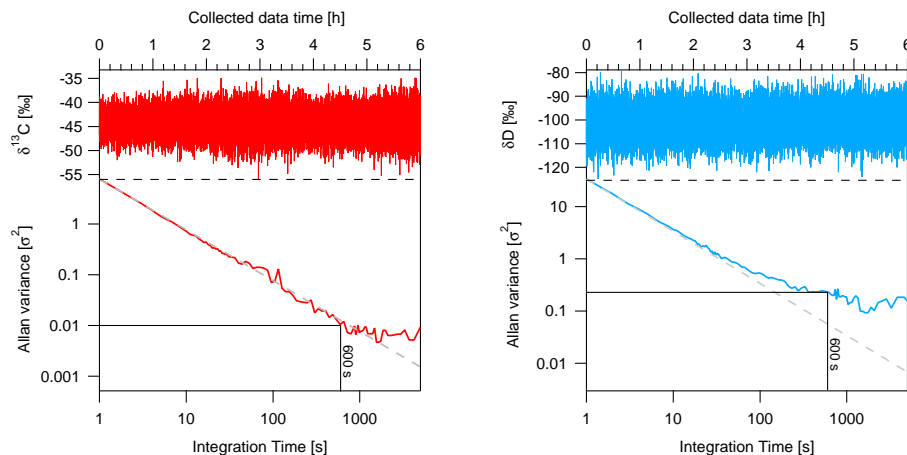


**Figure 5.** Allan variance plots for  $\delta^{13}\text{C}\text{-CH}_4$  (left) and for  $\delta\text{D}\text{-CH}_4$  (right) using 750 ppm  $\text{CH}_4$ . The upper plot shows the corresponding time series of  $\delta$ -values recorded at one second temporal resolution. At 600 s spectral averaging, the square root of the Allan variance indicates a precision of 0.1 ‰ for  $\delta^{13}\text{C}\text{-CH}_4$  and 0.5 ‰ for  $\delta\text{D}\text{-CH}_4$ .

## Real-time analysis of $\delta^{13}\text{C}$ - and $\delta\text{D}$ - $\text{CH}_4$ in ambient air with laser spectroscopy

S. Eyer et al.

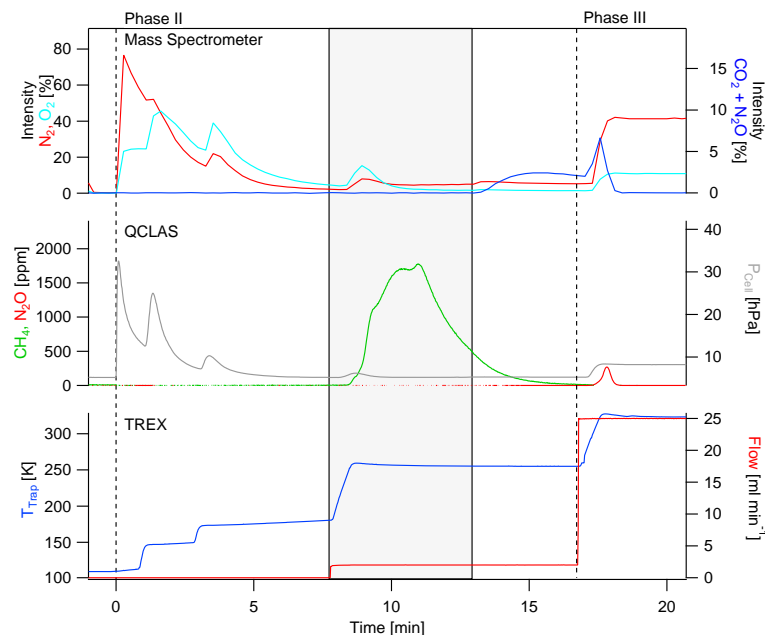


**Figure 6.** Phase II (desorption) and phase III (conditioning) of the  $\text{CH}_4$  preconcentration cycle by TREX. Mass spectrometer results (upper graph) indicate that the bulk gases  $\text{N}_2$  and  $\text{O}_2$  leave the trap shortly after decoupling the trap from the cold-plate and heating successively to 145 K (1 min) and 175 K (3 min), but a small reminder is also released in the main  $\text{CH}_4$  desorption step (see text for details). QCLAS measurements (middle graph) display that  $\text{CH}_4$  desorption is initiated by heating the trap to 258 K (8 min) and purging it with  $2 \text{ mL min}^{-1}$  synthetic air in forward flow direction; the gray shaded area indicates the period, during which the desorbed methane is filled into the gas cell of the laser spectrometer. In phase III (conditioning) the trap is heated up to 323 K and purged with  $25 \text{ mL min}^{-1}$  of high-purity synthetic air. The bottom graph exhibits the trap temperatures and flows of synthetic air in the preconcentration device (TREX).



## Real-time analysis of $\delta^{13}\text{C}$ - and $\delta\text{D-CH}_4$ in ambient air with laser spectroscopy

S. Eyer et al.

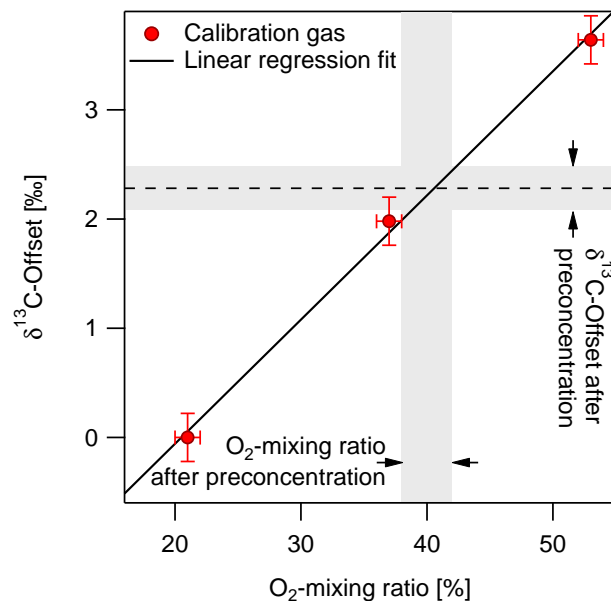


**Figure 7.**  $\delta^{13}\text{C}$ -offset as a function of  $\text{O}_2$  mole fraction determined from measurements of calibration gases without preconcentration with the QCLAS. This effect was found to be constant for  $\text{CH}_4$ -mole fractions from 600 to 1000 ppm. The grayed region shows the ranges of the  $\text{O}_2$ -mole fractions in the QCLAS-cell after preconcentration and the resulting offset in the  $\delta^{13}\text{C}$  values for typical TREX operation as determined from a series of experiments. The dashed horizontal line represents the offset in  $\delta^{13}\text{C}$  values of 2.3‰ used as a correction throughout the measurement campaign.

Title Page

Abstract

Introduction

Conclusions

References

Tables

Figures

◀

▶

◀

▶

Back

Close

Full Screen / Esc

Printer-friendly Version

Interactive Discussion



**Real-time analysis of  $\delta^{13}\text{C}$ - and  $\delta\text{D}$ - $\text{CH}_4$  in ambient air with laser spectroscopy**

S. Eyer et al.

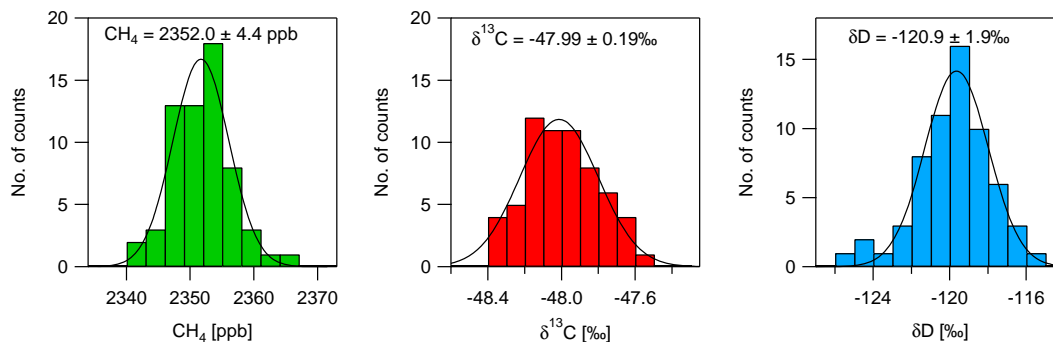


**Figure 8.** Repeated measurements of pressurized air (target gas) by TREX-QCLAS over two weeks throughout the interlaboratory comparison campaign. CH<sub>4</sub> mole fractions and relative differences of isotope ratios ( $\delta^{13}\text{C}$ ,  $\delta\text{D}$ ) were plotted as a histogram with bin widths of 3 ppb (CH<sub>4</sub>), 0.1‰ ( $\delta^{13}\text{C}$ ) and 1‰ ( $\delta\text{D}$ ), respectively. The uncertainty is given as the 1 $\sigma$  standard deviation.

[Title Page](#)[Abstract](#)[Introduction](#)[Conclusions](#)[References](#)[Tables](#)[Figures](#)[Back](#)[Close](#)[Full Screen / Esc](#)[Printer-friendly Version](#)[Interactive Discussion](#)

## Real-time analysis of $\delta^{13}\text{C}$ - and $\delta\text{D}$ - $\text{CH}_4$ in ambient air with laser spectroscopy

S. Eyer et al.

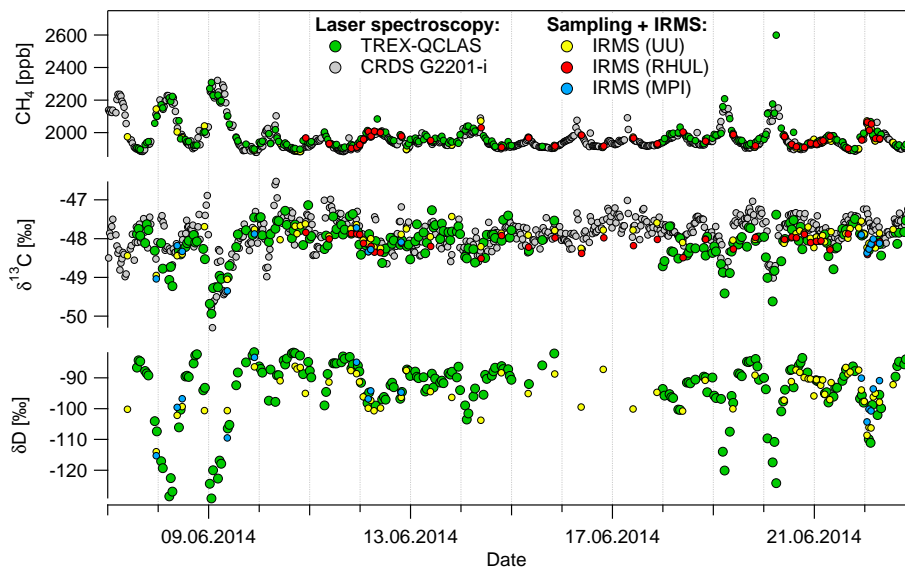


**Figure 9.**  $\text{CH}_4$  mole fractions and isotopic composition analyzed during the interlaboratory comparison campaign in real-time by the laser spectroscopic techniques: TREX-QCLAS ( $\text{CH}_4$ ,  $\delta^{13}\text{C}$ ,  $\delta\text{D}$ ), CRDS G2201-i ( $\text{CH}_4$ ,  $\delta^{13}\text{C}$ ), and on glass flask/bag samples with IRMS by UU ( $\text{CH}_4$ ,  $\delta^{13}\text{C}$ ,  $\delta\text{D}$ ), MPI ( $\text{CH}_4$ ,  $\delta^{13}\text{C}$ ,  $\delta\text{D}$ ) and RHUL ( $\text{CH}_4$ ,  $\delta^{13}\text{C}$ ).

[Title Page](#)[Abstract](#)[Introduction](#)[Conclusions](#)[References](#)[Tables](#)[Figures](#)[◀](#)[▶](#)[◀](#)[▶](#)[Back](#)[Close](#)[Full Screen / Esc](#)[Printer-friendly Version](#)[Interactive Discussion](#)

Real-time analysis of  $\delta^{13}\text{C}$ - and  $\delta\text{D-CH}_4$  in ambient air with laser spectroscopy

S. Eyer et al.

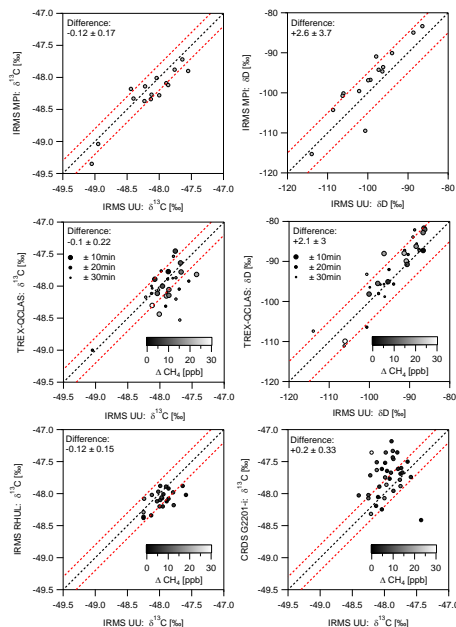


**Figure 10.** Correlation diagrams for  $\text{CH}_4$  isotope ( $\delta^{13}\text{C}$ ,  $\delta\text{D-CH}_4$ ) measurements in ambient air by different techniques and laboratories. The dashed black line is the 1 : 1 line, the red dashed lines indicate the WMO compatibility goals of  $\pm 0.2\text{‰}$  for  $\delta^{13}\text{C}$  and  $\pm 5\text{‰}$  for  $\delta\text{D}$ . Results of individual techniques are corrected to a common scale based on MPI results for a pressurized air target gas. For the middle and bottom graphs differences in  $\text{CH}_4$  mole fractions in gas samples are represented by the shading (black: identical mole fractions, white: 30 ppb difference). Top: IRMS analysis on glass flasks by the Stable Isotope Laboratory of MPI vs. UU for  $\delta^{13}\text{C-CH}_4$  (left) and  $\delta\text{D-CH}_4$  (right); Middle: TREX-QCLAS analysis by Empa vs. IRMS analysis on glass flasks by UU for  $\delta^{13}\text{C-CH}_4$  (left) and  $\delta\text{D-CH}_4$  (right). The temporal difference between TREX-QCLAS analysis and glass flask sampling is indicated by the point size (big:  $\pm 10$  min, medium:  $\pm 20$  min, small:  $\pm 30$  min); Bottom: IRMS analysis on bag samples by RHUL (left) and CRDS analysis by Eawag (right) vs. IRMS analysis on glass flasks by UU for  $\delta^{13}\text{C-CH}_4$ .

Title Page

Abstract

Introduction

Conclusions

References

Tables

Figures

◀

▶

◀

▶

Back

Close

Full Screen / Esc

Printer-friendly Version

Interactive Discussion



**Real-time analysis of  $\delta^{13}\text{C}$ - and  $\delta\text{D-CH}_4$  in ambient air with laser spectroscopy**

S. Eyer et al.

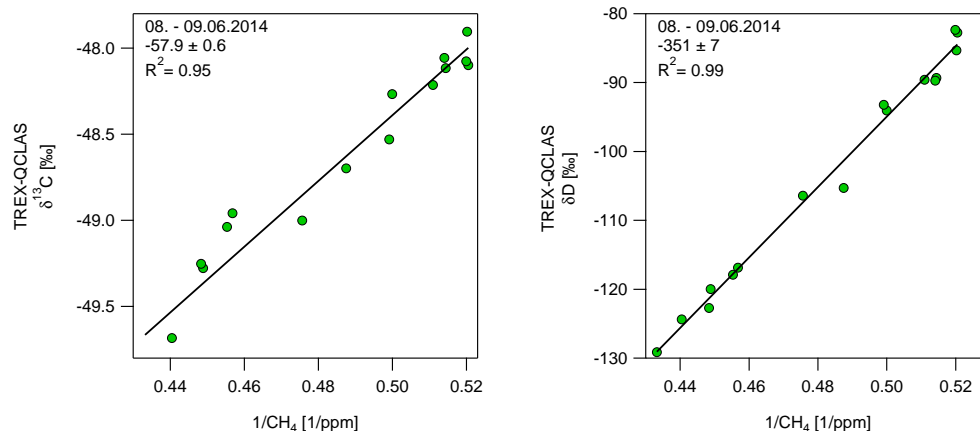


**Figure 11.** Representative Keeling plots for  $\delta^{13}\text{C-CH}_4$  and  $\delta\text{D-CH}_4$  for the period 8 June noon till 9 June 2014 noon. The isotopic source signature indicates a microbial origin, possibly referring to  $\text{CH}_4$  emissions from ruminants.

Title Page

Abstract

Introduction

Conclusions

References

Tables

Figures

◀

▶

◀

▶

Back

Close

Full Screen / Esc

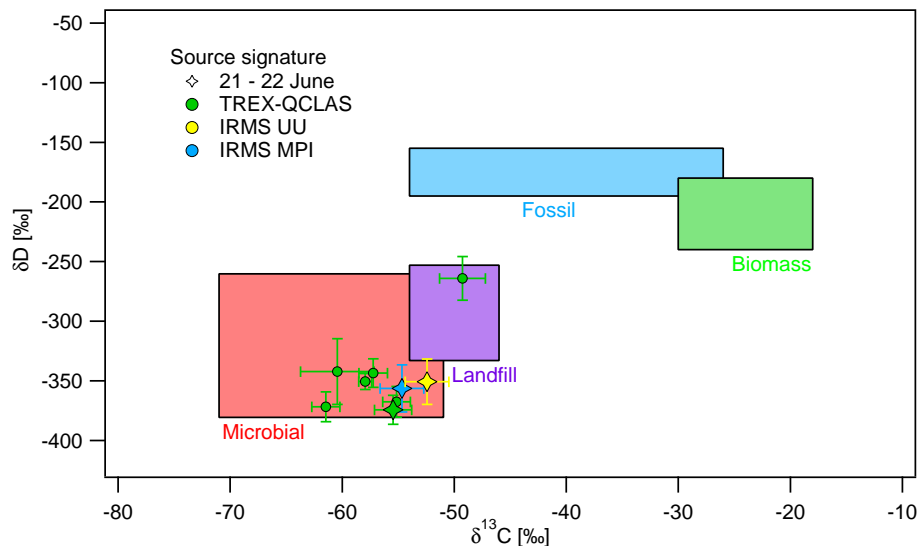
Printer-friendly Version

Interactive Discussion



**Real-time analysis of  $\delta^{13}\text{C}$ - and  $\delta\text{D}\text{-CH}_4$  in ambient air with laser spectroscopy**

S. Eyer et al.

[Title Page](#)[Abstract](#)[Introduction](#)[Conclusions](#)[References](#)[Tables](#)[Figures](#)[◀](#)[▶](#)[◀](#)[▶](#)[Back](#)[Close](#)[Full Screen / Esc](#)[Printer-friendly Version](#)[Interactive Discussion](#)

**Figure 12.**  $\delta\text{D}\text{-CH}_4$  vs.  $\delta^{13}\text{C}\text{-CH}_4$  of different  $\text{CH}_4$  sources. The symbols indicate  $\text{CH}_4$  source signatures derived from Keeling plots. The error bars are uncertainties derived from the linear regression. The star-symbols are source signatures from 21 June noon till 22 June noon derived from different techniques. The shadings indicate typical values for different source categories from the literature.